Dalton Transactions

ROYAL SOCIETY OF CHEMISTRY

PAPER

View Article Online
View Journal

Cite this: DOI: 10.1039/d6dt00680a

Insertion of $SnCl_2$ into the Pd–Cl bond: mechanistic elucidation and antitumor evaluation of trichlorostannyl palladium–NHC allyl complexes in ovarian cancer models

Eleonora Botter,[a] Valentina Lauteri,[a] Alessandro Rubbi,[b] Laura Orian,[b] Matteo Forner,[c] Valentina Gandin,[c] Nicola Demitri,[d] Vincenzo Canzonieri,[e,f] Flavio Rizzolio,[a,e] Enrico Cavarzerani,*[a] Fabiano Visentin *[a] and Thomas Scattolin *[b]

The development of effective and selective metal-based chemotherapeutics remains a central challenge in ovarian cancer treatment, particularly in addressing resistance to platinum agents. Herein, we report the design, synthesis, and biological evaluation of a novel series of heterobimetallic Pd(II)/Sn(II) η^3-allyl complexes bearing N-heterocyclic carbene (NHC) ligands. Thirteen complexes were efficiently prepared *via* $SnCl_2$ insertion into the Pd–Cl bond of allyl–palladium precursors, and fully characterized by NMR, IR, and X-ray diffraction. DFT calculations revealed a stepwise reaction mechanism initiated by a favourable Sn···Cl interaction, followed by insertion into the Pd–Cl bond. All compounds exhibited pronounced cytotoxicity across cisplatin-sensitive, cisplatin-resistant, and high-grade serous ovarian cancer (HGSOC) cell lines, with selected derivatives, particularly **2i** and **2k**, showing remarkable tumour selectivity. Lead compound **2i** retained potent activity in patient-derived tumour organoids (PDTOs), including a platinum-resistant model, while remaining inactive in a non-malignant fallopian tube epithelium organoid, highlighting its favourable therapeutic window. Mechanistic studies indicate that **2i** primarily targets thioredoxin reductase (TrxR) and mitochondria, as evidenced by early cytochrome c release and loss of mitochondrial membrane potential, with subsequent DNA damage occurring downstream, consistent with a mitochondria-driven apoptotic pathway distinct from classical platinum drugs. These findings position Pd(II)/Sn(II) η^3-allyl complexes, and **2i** in particular, as promising candidates for metal-based anticancer therapy.

Received 20th March 2026,
Accepted 24th March 2026

DOI: 10.1039/d6dt00680a

rsc.li/dalton

Introduction

Ovarian cancer remains one of the most lethal gynecological malignancies worldwide, with high-grade serous ovarian carcinoma (HGSOC) accounting for the majority of deaths.[1–3]

Its poor prognosis is largely attributable to the lack of early symptoms, with diagnosis frequently occurring only after extensive peritoneal dissemination. Standard therapy consists of surgery followed by platinum-based chemotherapy, most commonly cisplatin or carboplatin in combination with paclitaxel. Although initial responses may be favourable, relapse is frequent, and most patients eventually develop platinum-resistant disease.[4–7] At this stage, therapeutic options are extremely limited, and overall survival remains poor. This clinical scenario underscores the urgent need for novel chemotherapeutic strategies that exploit mechanisms different from those of platinum drugs.

In this context, organopalladium compounds have recently attracted attention as an emerging class of potential anticancer agents, particularly in ovarian cancer models.[8–31]

These compounds, which exhibit at least one strong Pd–C bond, are structurally versatile and can be designed to interact with a variety of biological targets. Their activity profiles often

[a]*Dipartimento di Scienze Molecolari e Nanosistemi, Università Ca' Foscari, Campus Scientifico Via Torino 155, 30174 Venezia-Mestre, Italy. E-mail: fvise@unive.it, enrico.cavarzerani@unive.it*
[b]*Dipartimento di Scienze Chimiche, Università degli Studi di Padova, via Marzolo 1, 35131 Padova, Italy. E-mail: thomas.scattolin@unipd.it*
[c]*Dipartimento di Scienze del Farmaco, Università degli Studi di Padova, via Marzolo 5, 35131 Padova, Italy*
[d]*Area Science Park, Elettra-Sincrotrone Trieste, S.S. 14 Km 163.5, Basovizza, 34149 Trieste, Italy*
[e]*Pathology Unit, Centro di Riferimento Oncologico di Aviano (C.R.O.) IRCCS, via Franco Gallini 2, 33081 Aviano, Italy*
[f]*Department of Medical, Surgical and Health Sciences, Università degli Studi di Trieste, Strada di Fiume 447, Trieste, Italy*

differ from those of classical platinum drugs, offering an opportunity to circumvent resistance pathways associated with DNA damage. Within this broad class, η^3-allyl palladium(II) complexes have shown particularly intriguing behavior.[22,26–29]

Evidence from very recent studies conducted by our group indicates that Pd(II)–allyl complexes can act as inhibitors of thioredoxin reductase (TrxR),[26,27] a selenoenzyme involved in maintaining the cellular redox balance.[32] TrxR is frequently overexpressed in ovarian cancer and contributes to tumor growth, metastatic progression, and chemoresistance.[33] Inhibition of this enzyme disrupts redox homeostasis, leading to increased intracellular levels of reactive oxygen species (ROS) and induction of apoptosis. Although this mechanism is not a general feature of all organopalladium compounds, it appears to represent a peculiar and significant mode of action for palladium–allyl derivatives.

The most promising and versatile palladium–allyl derivatives are those containing N-heterocyclic carbene (NHC) ligands and their derivatives.[22,26–29] Specifically, based on the formal charge at the metal center, these complexes can be broadly classified into three main categories: (i) neutral complexes of the type [Pd(NHC)Cl(allyl)], (ii) cationic $[Pd(NHC)(L)(allyl)]^+$ complexes (with L = 1,3,5-triaza-7-phosphaadamantane (PTA) being among the most relevant), and (iii) allyl palladates of the type $[NHC{\cdot}H][PdCl_2(allyl)]$, in which palladium bears a formal negative charge.

Our previous screening studies have shown that, for a given NHC-based ligand, neutral [Pd(NHC)Cl(allyl)] complexes are the least active, whereas cationic $[Pd(NHC)(L)(allyl)]^+$ species exhibit significantly higher cytotoxicity, which is generally comparable to, or slightly lower than, that of allyl palladates, the class that typically displays the lowest IC_{50} values.

Mechanistic investigations into these broad families of organopalladium derivatives have revealed that mitochondria are their primary cellular targets.[22,26–29] Damage to other cellular compartments occurs subsequently through a cascade process. At the molecular level, palladium–allyl complexes—regardless of their overall charge—have been shown to strongly inhibit thioredoxin reductase (TrxR).[26,27] Interestingly, the trend in cytotoxicity parallels that observed for TrxR inhibition: neutral [Pd(NHC)Cl(allyl)] complexes are weaker inhibitors (although comparable to the well-known TrxR inhibitor auranofin) than both cationic and anionic palladium allyl complexes.

Building on these observations, the reactivity of palladium–allyl complexes towards cysteine and selenocysteine residues located in the TrxR catalytic pocket has been investigated by DFT calculations, supported by ESI-MS studies.[15,34] These studies highlighted that the thiolate or selenolate preferentially attacks the metal center, leading to the formation of a new Pd–Se or Pd–S bond and displacement of the more labile ligand (chloride or PTA). This behaviour contrasts with that observed in some catalytic systems, where the allyl fragment itself is attacked, as exemplified by the Tsuji–Trost reaction.[35]

In the present study, we sought to explore whether the cytotoxicity—or at least the selectivity towards cancer cells—of the least active class of compounds, namely neutral [Pd(NHC)Cl(allyl)] complexes, could be enhanced by modifying their interaction with the molecular target, thioredoxin reductase (TrxR). Our strategy centered on replacing the chloride ligand with an anionic ligand featuring two key characteristics: (i) a stronger binding affinity for palladium than chloride, which could influence the reactivity pattern of the allyl fragment; and (ii) the presence of an additional metal center, enabling potential cooperative effects typical of heterobimetallic systems.

Based on these criteria, we selected the trichlorostannyl ($SnCl_3^-$) anion as the ligand. This species is known to be a strong σ-donor, with a bonding strength comparable to or even exceeding that of NHC ligands,[36] and its coordination introduces Sn(II) into the metal environment, thereby generating heterobimetallic Pd(II)/Sn(II) complexes.

It is worth noting that trichlorostannyl ligands have been widely investigated in coordination and organometallic chemistry. Numerous transition-metal complexes featuring M–$SnCl_3$ bonds have been structurally characterized, including derivatives of platinum-group metals.[37,38] For example, Albinati, Pregosin, and co-workers reported several Pt(II) complexes such as *trans*-$[Pt(SnCl_3)_2(P(OR)_3)_2]$ and related species, whose solid-state structures and multinuclear NMR properties demonstrated the pronounced *trans* influence and donor ability of the $SnCl_3^-$ ligand.[39] Similarly, Grassi, Musco and collaborators described η^3-allyl complexes of platinum and palladium containing a coordinated $SnCl_3$ group, providing crystallographic evidence for square-planar complexes of the type [M(η^3-allyl)($SnCl_3$)L] (M = Pd, Pt and L = CO, PR_3).[40–42] These studies are, however, rather dated, and the topic would benefit from a more up-to-date treatment.

Further examples of trichlorostannyl coordination have been reported for a range of transition metals, including rhodium,[37,43,44] iridium,[45–47] ruthenium,[48–52] and osmium,[53–55] thereby confirming that the $SnCl_3^-$ fragment is compatible with a wide variety of coordination environments.

Historically, the biological investigation of tin compounds has focused predominantly on Sn(IV) derivatives,[56] whereas Sn(II) species remain considerably underexplored. The few existing studies on Sn(II) compounds generally involve systems stabilized by strongly chelating ligands, such as pyridine-2-carboxaldehyde thiosemicarbazones,[57] or on stannocene derivatives.[58] This unbalanced distribution of research efforts is largely attributed to the pronounced hydrolytic sensitivity of Sn(II) in aqueous media, which compromises its stability under physiological conditions. Conversely, Sn(IV) complexes are typically more robust, and therefore more attractive for medicinal chemistry, particularly in the development of anticancer agents.[56]

In the present study, we sought to broaden the scope of tin-based therapeutics by exploring the use of Sn(II) in biological systems. To address its intrinsic instability, we adopted a stabilization strategy in which Sn(II) is incorporated as a trichlorostannyl ligand within a biologically active palladium–allyl complex. This design relies on the strong Pd–$SnCl_3$ bond, which is expected to help maintain both the oxidation state

and coordination environment of tin under biologically relevant conditions.

The most straightforward synthetic route to access such complexes involves the insertion of $SnCl_2$ into a Pd–Cl bond. Although this approach has been reported for other transition metals,[46,59–61] examples involving palladium remain relatively scarse.[62–64] More significantly, to the best of our knowledge, this strategy has not yet been applied to palladium complexes bearing NHC ligands. Consequently, the compounds described here represent the first examples of palladium complexes that incorporate both an NHC ligand and a trichlorostannyl ($SnCl_3$) fragment within the same coordination sphere. However, the mechanistic details of $SnCl_2$ insertion into Pd–Cl bonds remain largely unexplored.

Furthermore, metal complexes featuring a trichlorostannyl group—or stannyl complexes more broadly—have received limited attention in medicinal chemistry.[50,52,54] Nevertheless, a limited number of studies have examined the biological properties of coordination compounds containing $SnCl_3$ fragments. In particular, Blom and co-workers reported a series of half-sandwich ruthenium(II) and osmium(II) complexes bearing coordinated trichlorostannyl ligands, obtained *via* insertion of $SnCl_2$ into metal–chloride bonds, which were evaluated for antiproliferative activity against several human cancer cell lines (Fig. 1).[50,52,54,55] These studies showed that the presence of the $SnCl_3$ unit can significantly influence the cytotoxic profile of the resulting complexes, in some cases leading to activities comparable to or even exceeding those of reference metallodrugs such as cisplatin.

Related investigations have also considered coordination compounds containing $SnCl_3^-$ or $GeCl_3^-$ fragments either coordinated directly to the metal center or acting as counterions in salt-type complexes. Such systems were explored as a strategy to introduce group-14 elements into metal-based pharmacophores and to modulate their biological properties through heterometallic or ion-pair interactions.

Despite these encouraging preliminary results, the overall number of biologically investigated trichlorostannyl complexes remains very limited, and systematic studies addressing their mechanism of action, stability under physiological conditions, or potential cooperative effects between the transition metal and the Sn(II) center are still scarce. While these studies suggest promising biological activity, their scope and mechanistic insight remain limited, underscoring a significant knowledge gap.

In this context, the objectives of this study are twofold: first, to stabilize Sn(II) as a trichlorostannyl ligand coordinated to an allyl palladium–NHC scaffold; and second, to assess whether combining Pd(II) and Sn(II) within a single framework enhances antitumor activity or selectivity compared with analogous chloride-bearing Pd(II)–allyl complexes.

This design strategy is motivated by the potential of heterobimetallic complexes to exhibit biological properties superior to their mononuclear analogues. The presence of two distinct metal centers can induce cooperative effects—such as simultaneous interaction with different targets, modulation of redox behaviour, or fine-tuning of stability—that often result in improved cytotoxic profiles and selectivity.[65–67] Consequently, this approach offers a promising avenue for the development of chemotherapeutic candidates with capabilities extending beyond those of classical monometallic systems.

Results and discussion

Synthesis of trichlorostannyl palladium–NHC allyl complexes

The target trichlorostannyl palladium–NHC allyl complexes were successfully obtained *via* a two-step synthetic route, as depicted in Scheme 1.

The first step was the synthesis of [Pd(NHC)Cl(R-allyl)] precursors **1a–m**, which bear a wide range of NHC and allyl ligands. Specifically, when IPr, IMes, SIPr, and SIMes were selected as ancillary ligands (complexes **1a–g**), the well-known weak-base route was employed;[68] briefly, two equivalents of the desired imidazolium salt were reacted with the dimeric precursor [Pd(allyl)(μ-Cl)]$_2$ or its substituted analogues ([Pd(2-

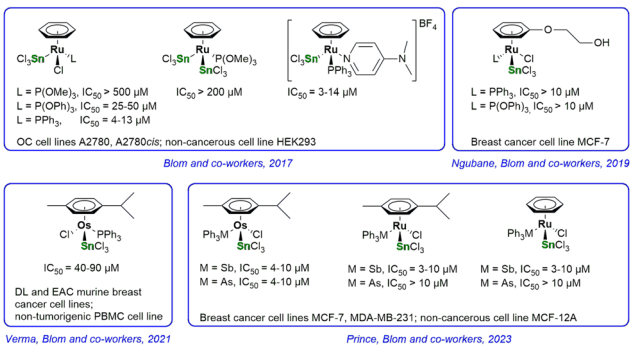

Fig. 1 Examples of trichlorostannyl complexes tested as anticancer agents.[50,52,54,55]

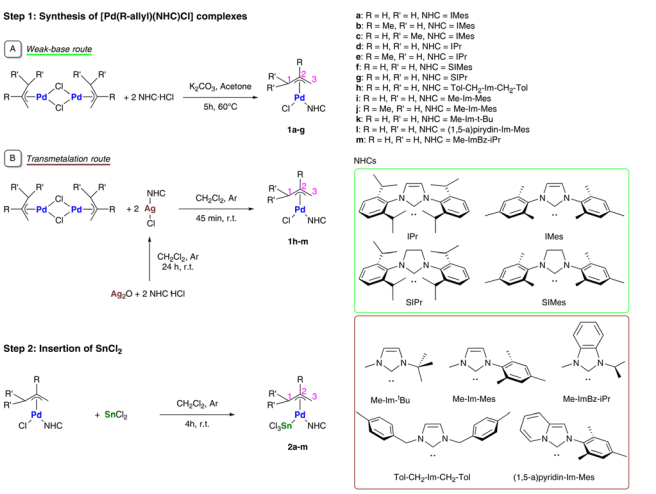

Scheme 1 Synthetic route to trichlorostannyl palladium–NHC allyl complexes.

methyl-allyl)(μ-Cl)]$_2$ or [Pd(1,1-dimethyl-allyl)(μ-Cl)]$_2$) in the presence of the K_2CO_3 as a weak base, using technical-grade acetone (green acetone) as solvent. The reaction mixture was stirred under aerobic conditions at 60 °C for 5 h. The desired [Pd(NHC)Cl(R-allyl)] complexes were then obtained by simple filtration of all the inorganic salts, followed by solvent removal under vacuum.

For the other NHCs, preliminary tests suggested that the transmetalation route was more suitable and led to the formation of a purer final product. This is likely ascribable to the lower steric demand of these carbene ligands. More specifically, this approach involved the reaction of the palladium dimer [Pd(allyl)(μ-Cl)]$_2$ (or [Pd(2-methyl-allyl)(μ-Cl)]$_2$) with a silver carbene complex, that had been previously synthesized according to the literature.[69] The transmetalation reaction proceeded smoothly at room temperature for 45 min in anhydrous dichloromethane and was accompanied by the precipitation of AgCl, which served as the main driving force of the process. The silver salt was easily removed by centrifugation and subsequent filtration through a pad of Celite (or a Millipore membrane), and the desired [Pd(NHC)Cl(R-allyl)] precursors **1h–m** were obtained by solvent removal under reduced pressure.

The second synthetic step involved the insertion of $SnCl_2$ into the Pd–Cl bond of the η^3-allyl palladium(II) precursors **1a–m**. The reaction was carried out by adding a slight excess (1.1 equiv.) of $SnCl_2$ to a dichloromethane solution of the Pd(II)–allyl precursor, stirring the mixture for 4 h at room temperature under an inert atmosphere. The excess of $SnCl_2$ ensured the complete conversion of the palladium precursors and was easily removed by filtration through a pad of Celite (or a Millipore membrane) due to its low solubility in CH_2Cl_2.

The target trichlorostannyl palladium–NHC complexes **2a–m** were isolated as microcrystalline powders in moderate to high yields (70–92%) after precipitation with diethyl ether or a diethyl ether/*n*-pentane mixture. The compounds were obtained in a sufficiently pure form, as confirmed by the results of elemental analyses.

The formation of the desired complexes was confirmed initially by NMR spectroscopy. In the ^{1}H NMR spectra, five distinct resonances attributable to the η^3-allyl fragment are observed. In particular, the signal of H^2, directly bound to the central carbon atom of the allyl group, appears at 4.5–5.0 ppm. Two sets of diastereotopic resonances are detected for H^1 and H^3: the *syn*-H$^{1/3}$ protons resonate at 4.0–4.5 ppm, whereas the *anti*-H$^{1/3}$ protons are found at 2.0–2.5 ppm. The differentiation between *syn* and *anti* protons is fully consistent with the geometry of the Pd–allyl scaffold, which is known to adopt a conformation nearly perpendicular to the coordination plane of the complex, with a deviation of approximately 5–10° from ideal orthogonality.[70]

The presence of two different signals for H^1 and H^3 also provides indirect evidence of the inequivalence of the two ancillary ligands (NHC and $SnCl_3^-$) at the palladium center. Notably, both *syn*-H^3 and *anti*-H^3 display satellite peaks arising from coupling with ^{117}Sn and ^{119}Sn nuclei, thereby confirming the coordination of the trichlorostannyl ligand to the metal center.

These protons are markedly downfield-shifted relative to the corresponding signals in the [Pd(NHC)Cl(R-allyl)] precursors, an effect attributable to the stronger *trans*-labilising ability of $SnCl_3^-$ compared to chloride. This trend is most pronounced for H^3, positioned *trans* to the trichlorostannyl ligand.

Consistent with the ^{1}H NMR data, the ^{13}C{^{1}H} NMR spectra show a substantial downfield shift of C^3, resonating approximately 20 ppm higher than in the chlorinated analogue. Remarkably, C^1 resonates in close proximity to C^3, at around 70 ppm, suggesting that the *trans*-labilising influence of $SnCl_3^-$ is comparable to that of the NHC ligand.

A complete assignment of all proton and carbon resonances was achieved with the aid of 2D NMR experiments, including COSY, HMQC, HMBC, and NOESY.

For complex **2k**, featuring Me-Im-^{t}Bu as the ancillary ligand, two distinct isomers are observed at room temperature. The significant steric bulk of the *tert*-butyl substituent in this unsymmetrical NHC ligand restricts rotation around the Pd–C^{NHC} bond. In combination with the inequivalence of the two ligands at the metal center (the η^3-allyl fragment and the $SnCl_3^-$ ligand), this constraint leads to the formation of two stereoisomers, readily distinguished in the NMR spectra by the presence of two distinct sets of resonances.

It is well established that increasing the temperature, as well the introduction of nucleophiles and/or polar solvents, promotes *syn–anti* isomerization in this class of complexes *via* formation of a Pd–η^1-allyl intermediate, which rapidly rearranges to the thermodynamically favoured Pd–η^3-allyl species.[71–73]

In the case of **2m**, bearing Me-BzIm-^{i}Pr as the ancillary ligand, rotation around the Pd–C^{NHC} bond is only partially restricted at room temperature, as evidenced by the broad resonances observed in the ^{1}H NMR spectra. Upon cooling to 253 K, two distinct isomers become clearly distinguishable. This behaviour is consistent with the reduced steric demand of the ^{i}Pr group compared to ^{t}Bu.

Interestingly, for **2c**—where two isomers are theoretically feasible based on the relative orientation of the methyl substituent on the allyl moiety and the two different ancillary ligands—only a single isomer is detected. The observed species corresponds to the configuration in which the unsubstituted allyl carbon lies *trans* to the trichlorostannyl ligand. This assignment is corroborated by the presence of two $^{117/119}$Sn satellite peaks associated with the *syn*-H^3 proton.

Further characterization was conducted *via* IR spectroscopy, providing additional confirmation of $SnCl_3$ coordination. Specifically, two absorption bands are observed at 300–330 cm^{-1}, which are absent in the IR spectra of the [Pd(NHC)(allyl)Cl] precursors. These features are assignable to the symmetric and asymmetric Sn–Cl stretching modes.[62]

Finally, the molecular structures of complexes **2b**, **2d**, and **2f** were unambiguously determined by single-crystal X-ray diffraction (Fig. 2). Suitable crystals were obtained by slow diffusion of diethyl ether into dichloromethane (or chloroform) solutions of the complexes at 4 °C.

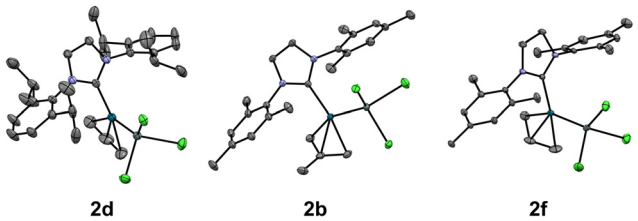

Fig. 2 XRD structure of complexes **2d**, **2b** and **2f** at 100 K. Hydrogen atoms and solvent molecules are omitted.

Specifically, complexes **2b**, **2d** and **2f** show square planar palladium(II) and tetrahedral tin(II) coordination spheres (Tables S2–S4 in the SI). Steric hindrance of bulky trichlorostannyl ligand maintains the Pd(II) coordination plane almost perpendicular to the NHC ring, as previously reported in two examples of Pd–Sn complexes (CCDC 2291609[74] and 2250762[75]). Allyl ligand substituents are able to influence this parameter, which is significantly reduced (~60°) in **2b** (shown with cyan sticks in Fig. S3) due to formation of an intramolecular CH···π interaction, blocking η^3-coordination in a well-defined orientation. Crystal packing shows hydrophobic contacts among neighbour molecules, through weak intermolecular CH···π interactions, involving NHC substituents. Dichloromethane solvent molecules have been found in the crystal packing of **2b** (Fig. S1A–C). Minor cell volume contraction has been found in **2b** and **2f** (~4%) upon cooling, with no significant packing and molecular rearrangements, as shown through the models' overlap (Fig. S2; R.M.S.D. <0.2 Å).

One of the most relevant structural parameters is the distance between the palladium centre and the two terminal allyl carbon atoms. In the heterobimetallic Pd(II)/Sn(II) complexes targeted in this study, the Pd–C distances to the two terminal allyl carbons are very similar (*ca.* 2.17–2.18 Å), indicating a comparable *trans* influence of the NHC and trichlorostannyl ligands. Conversely, crystallographic data reported in the literature for monometallic [Pd(NHC)Cl(allyl)] complexes show a significantly shorter Pd–C distance for the allyl carbon *trans* to the chloride than for that *trans* to the carbene (*ca.* 2.10 *vs.* 2.20 Å, respectively).[76] This observation clearly supports the substantially stronger *trans*-labilising character of NHC ligands compared to chloride.

Mechanism of $SnCl_2$ insertion into the Pd–Cl bond

The mechanism of the insertion reaction of $SnCl_2$ with η^3-allyl–NHC palladium complexes was studied *in silico* by DFT at the COSMO-ZORA-M06/TZ2P-ae//COSMO-ZORA-BLYP-D3(BJ)/TZP level of theory. Compounds **1a** and **1k** were evaluated to assess the effect of different carbene moieties on the energy profiles.

The insertion reactions begin with the formation of energetically favourable reactant complexes (RCs), in which $SnCl_2$ coordinates to the chloride ligand of **1a** and **1k** (**1a-RC** and **1k-RC**) (Scheme 2). As the Pd–Cl bond is gradually stretched, allowing $SnCl_2$ to approach the Pd center, the adducts deformed into triangle-shaped transition state (TS) geometries (**1a-TS** and **1k-TS**). The insertion products are formed in a single concerted step, with Sn adopting a tetrahedral coordination geometry.

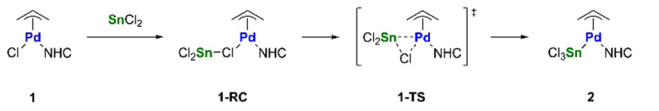

Scheme 2 Proposed insertion mechanism of $SnCl_2$ into the Pd–Cl bond.

Table 1 reports the Gibbs free energies of the stationary points shown in Fig. 3. Both reactant complexes, **1a-RC** and

Table 1 Gibbs free energies (kcal mol^{-1}) for the reaction of **1a** and **1k** with $SnCl_2$ in CH_2Cl_2: energies of reactant complexes ($\Delta G_{1\text{-RC}}$), transition states ($\Delta G_{1\text{-TS}}$) and products (ΔG_2) relative to the free reactants

	$\Delta G_{1\text{-RC}}$	$\Delta G_{1\text{-TS}}$	ΔG_2
1a + $SnCl_2$	−8.8	3.1 (11.9)	−7.8
1k + $SnCl_2$	−8.2	0.3 (8.5)	−10.3

Activation energies relative to the reactant complexes are given in brackets. Level of theory: COSMO-ZORA-M06/TZ2P-ae//COSMO-ZORA-BLYP-D3(BJ)-TZP.

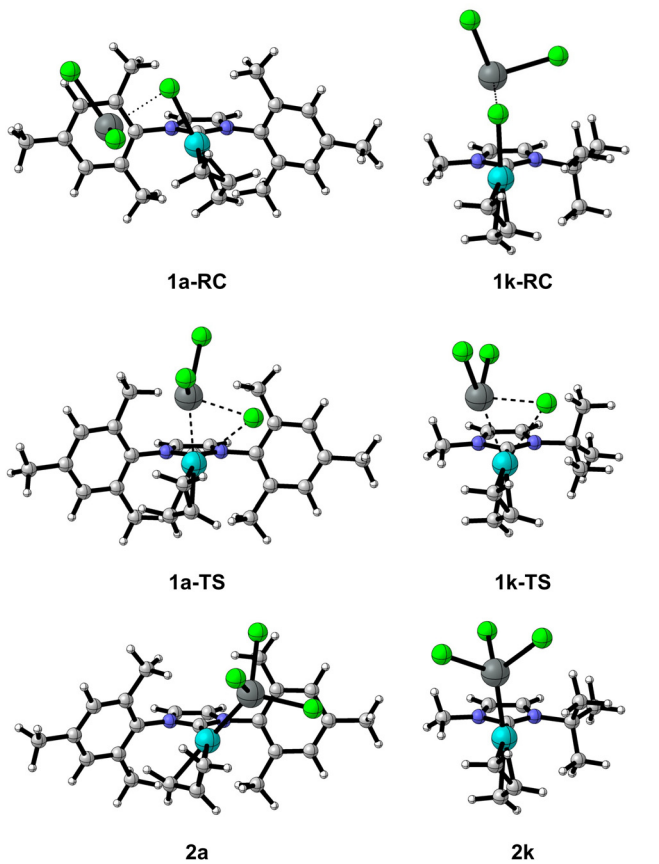

Fig. 3 Reactant complexes (RC), transition states (TS) and products for the reaction of **1a** and **1k** with $SnCl_2$ in CH_2Cl_2 (Pd, cyan; Cl, green; Sn, grey). Level of theory: COSMO-ZORA-BLYP-D3(BJ)/TZP.

1k-RC, are approximately 8 kcal mol^{-1} more stable than the free reactants. Consequently, the activation energy for the insertion is increased and is highest for **1a** (11.9 kcal mol^{-1} for **1a** *vs.* 8.5 kcal mol^{-1} for **1k**). Although the overall reaction is exergonic, the products are not significantly more stable than their corresponding RCs. In fact, the relative energy of **2a** is computed to be 1.0 kcal mol^{-1} higher than **1a-RC**. The formation of **2a** is both thermodynamically and kinetically less favourable than that of **2k**, most likely a result of the greater steric demand of the carbene ligands in **1a**.

In vitro cytotoxicity on human ovarian cancer cell lines

As mentioned in the Introduction, despite the longstanding clinical success of platinum-based chemotherapeutics, the emergence of resistance and dose-limiting toxicity continue to drive the search for alternative metal-based agents for the treatment of ovarian cancer. In this context, palladium(II) η^3-allyl complexes have recently attracted considerable attention, having demonstrated compelling antiproliferative activity across a range of cancer models, including ovarian cancer (OC) and high-grade serous ovarian cancer (HGSOC) cell lines.

On the basis of these promising precedents, and after confirming compound stability in a DMSO-d_6/D_2O medium, we evaluated the *in vitro* anticancer activity of the newly synthesized heterobimetallic Pd(II)/Sn(II) complexes. The biological assessment was carried out on a representative panel of human ovarian cancer cell lines encompassing both cisplatin-sensitive and cisplatin-resistant phenotypes: A2780, its cisplatin-resistant variant A2780*cis*, and two HGSOC-derived models, OVCAR-5 and KURAMOCHI. To preliminarily assess tumour selectivity, cytotoxicity was also evaluated in the non-cancerous human lung fibroblast cell line MRC-5.

Cells were treated with increasing concentrations of the complexes (0.001–100 μM) for 96 h, after which cell viability was quantified and IC_{50} values were calculated from the corresponding dose–response curves. Cisplatin was used as a benchmark compound and evaluated in parallel under identical experimental conditions.

The resulting cytotoxicity profiles are summarized in Table 2.

All the complexes displayed cytotoxic activities against the A2780 ovarian cancer cell line comparable to that of cisplatin, with the sole exception of complex **2k**, which exhibited a significantly higher IC_{50} value, albeit still within the micromolar range. Importantly, the pronounced antiproliferative activity of our heterobimetallic Pd(II)/Sn(II) complexes was fully retained in the cisplatin-resistant A2780*cis* clone, indicating a potential ability to circumvent the resistance mechanisms that limit the efficacy of classical platinum-based chemotherapeutics. Notably, in A2780*cis* cells, the newly synthesized complexes were at least one order of magnitude more active than cisplatin.

Encouraging results were also obtained in the high-grade serous ovarian cancer cell line KURAMOCHI, where IC_{50} values were in most cases comparable to, or lower than, those measured in the more conventional A2780 and A2780*cis* models. Once again, compound **2k** emerged as the least active derivative within the series, an effect that may be tentatively attributed to the presence of two alkyl *N*-substituents on the imidazole ring, a structural feature unique to this ligand among those investigated.

In contrast, a marked decrease in cytotoxic activity was observed in the OVCAR-5 cell line for the majority of the complexes, underscoring the intrinsic resistance of this HGSOC model. Notably, this effect was significantly attenuated for compounds **2a**, **2f**, **2g**, **2h**, **2l** and **2m**. With the exception of **2a** and **2h**, all these derivatives feature a coordinated N-heterocyclic carbene ligand derived from a non-imidazole scaffold, suggesting that variations in carbene architecture may modulate the activity in this particularly refractory cellular context.

Table 2 IC_{50} values of the newly synthesized heterobimetallic Pd(II)/Sn(II) complexes after 96 hours of incubation

	IC_{50} (μM)					
Complex	A2780	A2780*cis*	OVCAR-5	KURAMOCHI	MRC-5	SI
Cisplatin	0.30 ± 0.07	7.2 ± 0.8	0.54 ± 0.09	0.59 ± 0.02	1.7 ± 0.3	0.8
2a	0.29 ± 0.04	0.16 ± 0.06	0.8 ± 0.2	0.10 ± 0.06	0.35 ± 0.08	1
2b	0.4 ± 0.1	0.37 ± 0.07	3.6 ± 0.3	0.07 ± 0.04	0.36 ± 0.06	0.3
2c	0.18 ± 0.01	0.2 ± 0.1	1.1 ± 0.3	0.029 ± 0.002	0.037 ± 0.002	0.09
2d	0.20 ± 0.07	0.24 ± 0.05	4.2 ± 0.2	0.08 ± 0.03	0.7 ± 0.3	0.6
2e	0.4 ± 0.2	0.3 ± 0.1	3.9 ± 0.3	0.051 ± 0.006	0.13 ± 0.02	0.1
2f	0.28 ± 0.08	0.09 ± 0.04	0.47 ± 0.07	0.042 ± 0.004	0.26 ± 0.06	1
2g	0.52 ± 0.07	0.27 ± 0.05	0.84 ± 0.07	0.06 ± 0.02	0.8 ± 0.2	2
2h	0.4 ± 0.1	0.32 ± 0.07	0.31 ± 0.02	0.39 ± 0.03	3.6 ± 0.1	10
2i	0.4 ± 0.1	0.10 ± 0.06	3.3 ± 0.1	0.30 ± 0.02	>100	>99
2j	0.39 ± 0.07	0.26 ± 0.06	5.5 ± 0.3	0.25 ± 0.02	11 ± 4	7
2k	2.5 ± 0.4	0.5 ± 0.3	4.4 ± 0.2	4.4 ± 0.2	>100	>34
2l	0.3 ± 0.1	0.3 ± 0.1	0.63 ± 0.06	0.22 ± 0.01	2.3 ± 0.5	6
2m	0.16 ± 0.08	0.3 ± 0.1	0.19 ± 0.02	0.21 ± 0.04	3.0 ± 0.1	14
1i	0.41 ± 0.02	0.38 ± 0.04	3.9 ± 0.4	0.55 ± 0.05	20 ± 8	15

For each complex, a stock solution 10 mM in DMSO was used, while for cisplatin a stock solution 3.33 mM in water was used. A2780 and A2780*cis* (cisplatin-sensitive and cisplatin-resistant OC cells), OVCAR-5 and KURAMOCHI (HGSOC), and MRC-5 (normal lung fibroblasts).

Taken together, these data indicate that the nature of the NHC ligand coordinated to palladium exerts only a limited influence on the overall anticancer activity across the four ovarian cancer cell lines examined. A similar conclusion can be drawn for substitution at the η^3-allyl fragment: methyl substitution at either the C^1 or C^2 position does not significantly affect the cytotoxic effect, as reflected by the closely comparable IC_{50} values observed for complexes **2a–2c** and for complexes **2i** and **2j**, which bear the same NHC ligand and differ exclusively in the allyl substitution pattern.

The overall antiproliferative activity of the present complexes is comparable to that of the most effective η^3-allyl palladium systems reported to date,[19,22,77–79] and clearly surpasses that of less active organometallic motifs, such as palladacyclopentadienyl and Pd(0)–olefin derivatives.[30,80] These observations further highlight the central role of the Pd(II)–allyl fragment as a key pharmacophoric unit governing cytotoxicity within this class of compounds.

A markedly different trend emerges when cytotoxicity is evaluated in non-cancerous MRC-5 human lung fibroblasts. While several complexes display similar toxicity towards normal and cancerous cells, a pronounced reduction in cytotoxicity—often exceeding one order of magnitude in IC_{50} values—is observed for complexes **2h–2m**, thereby indicating a substantial degree of tumour selectivity within this subset. In particular, compounds **2l** and **2m** incorporate NHC ligands based on imidazopyridine and benzimidazole scaffolds, respectively, which distinguish them from the other carbenes examined and may account for their divergent biological behaviour in normal cells. For complexes **2h–2k**, the enhanced selectivity may instead be related to the presence of an alkyl substituent on at least one of the nitrogen atoms of the carbene ligand, a feature not shared by all imidazole-based NHCs in this series.

Remarkably, the highest selectivity indices were observed for complexes **2i** and **2k** (with SI >99 and >34, respectively), both bearing an NHC ligand with a methyl substituent. Among them, compound **2i** stood out as the most promising candidate, as it combines a generally higher cytotoxic activity against ovarian cancer cells than cisplatin, with an approximately two-orders-of-magnitude greater selectivity towards tumour cells, thereby identifying it as a particularly attractive lead for further development.

Interestingly, these observations were further reinforced by comparison with the corresponding monometallic [Pd(NHC)Cl(allyl)] precursor **1i**. Although **1i** displayed cytotoxic activity against ovarian cancer cells comparable to that of its trichlorostannyl analogue **2i**, it also exhibited a non-negligible cytotoxicity towards non-cancerous MRC-5 cells, resulting in a substantially lower selectivity index. In contrast, insertion of $SnCl_2$ to form trichlorostannyl derivative **2i** markedly attenuates the cytotoxic effects in normal cells while fully preserving its high anticancer activity. Taken together, these findings highlight the key role of the trichlorostannyl ligand in modulating the biological profile of allylpalladium–NHC complexes and demonstrate, in the case of the lead compound of this study, that $SnCl_2$ insertion constitutes an effective strategy for enhancing tumour selectivity relative to the monometallic precursor [Pd(NHC)Cl(allyl)].

Ex vivo anticancer activity on 3D patient-derived tumoroids

While conventional two-dimensional (2D) cell culture models remain indispensable for the preliminary assessment of anticancer activity, they fail to capture the structural, biochemical, and functional complexity of solid tumours. In particular, 2D systems fail to recapitulate the intricate cell–cell and cell–matrix interactions that critically regulate tumour growth, survival, and therapeutic response, thereby often leading to an overestimation of drug efficacy. To bridge this gap, three-dimensional (3D) culture platforms have been increasingly adopted in drug discovery pipelines.[81,82] Among these, multicellular spheroids represent an important advancement over traditional monolayer cultures. However, their limited cellular heterogeneity, lack of long-term genetic stability, and simplified architecture restrict their predictive power.

In contrast, patient-derived tumour organoids (PDTOs) have emerged as highly advanced and physiologically relevant *ex vivo* models, capable of faithfully reproducing the histo-architectural organization, cellular diversity, and key molecular features of the original tumour tissue. Unlike spheroids, organoids self-organize into complex 3D structures, preserve tumour-specific genetic and phenotypic traits over extended culture periods, and retain key features of the tumour microenvironment that regulate therapeutic sensitivity and resistance. As a result, PDTOs have demonstrated a remarkable ability to predict patient-specific drug responses, in some cases outperforming traditional *in vivo* models in terms of translational relevance, scalability, and ethical sustainability.[83–86] Consequently, organoid-based platforms are now widely regarded as among the most reliable preclinical models for anticancer drug screening and personalized medicine.[87]

The adoption of such clinically relevant models is particularly important for metal-based compounds, whose biological activity is highly sensitive to microenvironmental parameters such as redox state, extracellular matrix composition, and cell–cell interactions. Evaluating these agents in systems that closely mimic *in vivo* tumour conditions is therefore essential to obtain meaningful insights into their therapeutic potential.

Based on the *in vitro* results, compound **2i**, which combines high cytotoxic potency with marked tumour selectivity, was selected for evaluation in ovarian cancer PDTOs. Specifically, two patient-derived tumour organoids (HGSOC-PDTO-1 and HGSOC-PDTO-2), recently established in our laboratory from high-grade serous ovarian cancer (HGSOC) specimens, were employed. Previous immunohistochemical characterization confirmed that these tumour organoids retained the key histopathological features of the corresponding primary tumours, including robust expression of clinically relevant markers such as PAX8, WT-1, and CA-125.

As a non-cancerous control, compound **2i** was also tested against a mouse-derived fallopian tube epithelium organoid (FTE-MDO), generated from healthy ovarian tissue.

Table 3 IC_{50} values calculated for complex **2i** when tested on patient-derived HGSOC and mouse-derived fallopian tube epithelium organoids

	IC_{50} (μM)		
Organoid	Carboplatin	Doxorubicin	**2i**
HGSOC-PDTO-1	17 ± 9	38 ± 9	5 ± 1
HGSOC-PDTO-2	>200	2 ± 1	2 ± 1
FTE-MDO	21 ± 9	2.2 ± 0.5	>200

Results were obtained after 96 hours of incubation with complex solutions ranging from 200 μM to 0.0256 μM, prepared from a stock solution 10 mM in DMSO. For carboplatin and doxorubicin stock solutions respectively 10 mg mL^{-1} and 2 mg mL^{-1} in water were used.

The IC_{50} values reported in Table 3 demonstrate a pronounced antiproliferative activity of compound **2i** in HGSOC-PDTO-1, with potency slightly exceeding that of the clinically used agents carboplatin and doxorubicin, which were included as reference compounds. Notably, comparable activity was also observed in HGSOC-PDTO-2, a model that displays sensitivity to doxorubicin but resistance to carboplatin. These findings further support the hypothesis that the Pd(II)-based complex may overcome resistance mechanisms commonly associated with platinum-based drugs.

Importantly, the strong tumour selectivity observed in 2D cell-based assays is preserved in the organoid model. In fact, compound **2i** shows no detectable cytotoxicity towards the non-cancerous FTE-MDO, in sharp contrast to carboplatin and doxorubicin, which display appreciable toxicity in this healthy tissue-derived system. This result underscores the favourable therapeutic profile of compound **2i** and highlights the power of organoid-based screening in discriminating between efficacy and off-target toxicity within a clinically meaningful context.

Mechanism of action and cell death

Motivated by the exceptional antiproliferative potency and tumour selectivity exhibited by compound **2i**, we next sought to elucidate its mechanism of action at the cellular level.

On the basis of our previous studies, which identified mitochondria as preferential intracellular targets of η^3-allyl palladium(II) complexes bearing N-heterocyclic carbene ligands,[22] we hypothesised that compound **2i** primarily disrupts mitochondrial function, thereby activating downstream cell death pathways rather than directly targeting nuclear DNA.

To investigate this hypothesis, we performed time-resolved immunofluorescence analyses focusing on two well-established hallmarks of cytotoxic stress: cytochrome c release and DNA double-strand break (DSB) formation.

We first investigated the intracellular distribution of cytochrome c, a small heme protein located in the mitochondrial intermembrane space that plays a central role in oxidative phosphorylation under physiological conditions. Upon mitochondrial outer membrane permeabilisation (MOMP), cytochrome c is released into the cytosol, where it contributes to apoptosome assembly and initiates the intrinsic apoptotic cascade.[88] Consequently, immunofluorescence-based detection of cytochrome c redistribution from a punctate, mitochondria-confined pattern to a diffuse cytosolic signal is widely recognised as a robust indicator of mitochondrial damage and apoptotic commitment.

From an experimental standpoint, A2780 ovarian cancer cells were treated with compound **2i** at sub-micromolar concentrations (0.5 and 1.0 μM) or with cisplatin (10 μM) as a reference DNA-damaging agent, and analysed after 3, 6, 24, and 48 h of exposure. Immunofluorescence imaging (Fig. 4a) revealed that treatment with compound **2i** induced a pronounced time-dependent release of cytochrome c, which became clearly detectable after 24 h. A similar redistribution was observed in cisplatin-treated cells, albeit at substantially higher concentrations. These results indicate that compound **2i** effectively compromises mitochondrial integrity and triggers mitochondria-mediated apoptotic signalling at doses an order of magnitude lower than those required for cisplatin.

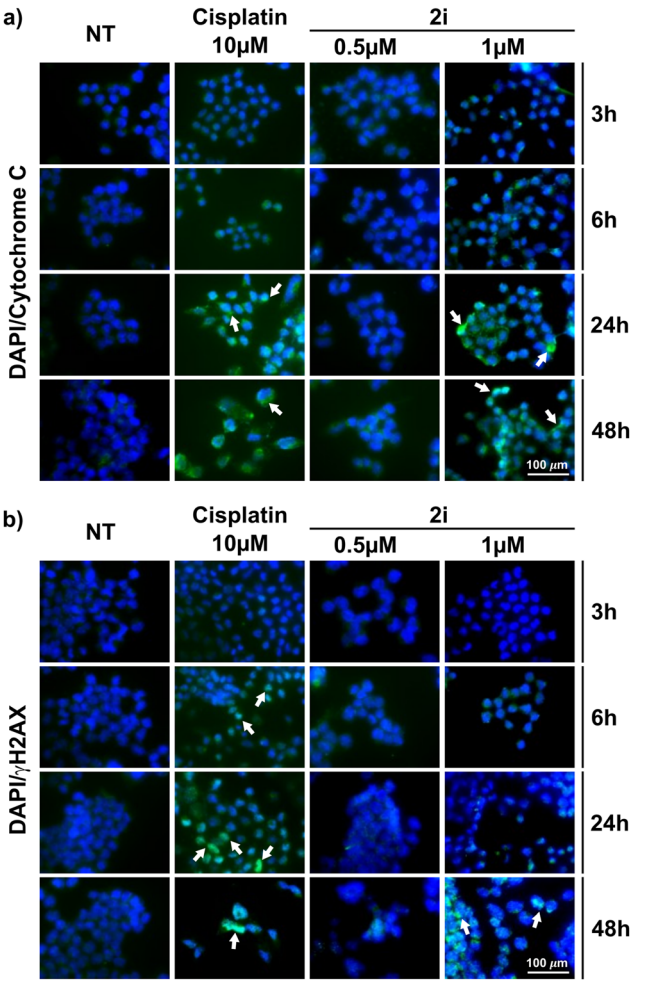

Fig. 4 Immunofluorescence analysis of (a) cytochrome c release, and (b) histone H2AX phosphorylation. For both experiments, A2780 cells were incubated for 3, 6, 24 and 48 hours with complex **2i** (concentration 0.5 and 1.0 μM) and cisplatin (positive control – concentration 10 μM). Arrows indicated cytochrome c release and DNA damage, respectively.

To establish whether nuclear DNA constitutes a primary molecular target of compound **2i** or is instead affected as a downstream consequence of mitochondrial dysfunction, we assessed DNA damage using the γH2AX immunofluorescence assay. Phosphorylation of the histone variant H2AX at serine 139 (γH2AX) represents one of the earliest cellular responses to DNA double-strand breaks and leads to the rapid formation of discrete nuclear foci at sites of DNA damage.[89] The detection and quantification of γH2AX foci therefore provide a highly sensitive and reliable readout of the presence, extent, and persistence of DSBs, as well as for the activation of DNA damage response and repair pathways.[90]

In agreement with its well-established mechanism of action, cisplatin induces rapid γH2AX phosphorylation, with clear foci formation observable as early as 6 h post-treatment and progressively increasing at 24 and 48 h (Fig. 4b), reflecting the accumulation of unrepaired DNA lesions resulting from platinum–DNA adduct formation. In striking contrast, compound **2i** does not induce significant γH2AX signalling at early time points, with appreciable DSB formation becoming evident only after prolonged exposure (48 h).

The clear temporal separation between mitochondrial dysfunction and DNA damage provides compelling evidence that mitochondrial impairment represents the primary cytotoxic event induced by compound **2i**, whereas DNA damage likely arises as a secondary consequence of apoptotic progression. This mitochondria-centered mechanism of action clearly differentiates compound **2i** from classical platinum-based chemotherapeutics and provides a mechanistic rationale for its retained efficacy in cisplatin-resistant ovarian cancer models.

TrxR plays a crucial role in maintaining mitochondrial integrity and inhibiting apoptosis by regulating the redox state of cytochrome c and preventing its release. Upon inhibition, the resulting loss of cellular antioxidant capacity causes excessive ROS production, mitochondrial membrane permeabilization, and the leakage of cytochrome c into the cytosol, triggering apoptosis. Based on the established connections between TrxR and mitochondria-driven apoptosis, and considering our recent identification of unprecedented palladium complexes capable of targeting TrxR,[26] we evaluated the ability of compound **2i** to inhibit TrxR in both a cell-free system and in human ovarian cancer cells. Auranofin, a well-known metal-based TrxR inhibitor, was used as a positive control and TrxR activity was assayed by measuring the NADPH-dependent reduction of DTNB at 412 nm, as described in the Experimental section.

In cell-free assays, compound **2i** exhibited a dose-dependent inhibition of TrxR activity, with an IC_{50} value of 46 nM, approximately two orders of magnitude higher than that observed for auranofin, that elicited an IC_{50} value of 0.4 nM (Fig. 5A). Conversely, in human ovarian cancer A2780 cells, **2i** displayed a more pronounced inhibitory effect on TrxR, with a potency comparable to that of auranofin (Fig. 5B). Notably, IC_{50} values of 1.6 and 1.8 μM were determined for **2i** and auranofin, respectively.

Cellular TrxR inhibition, particularly the mitochondrial isoform TrxR2, represents a potent mechanism for disrupting

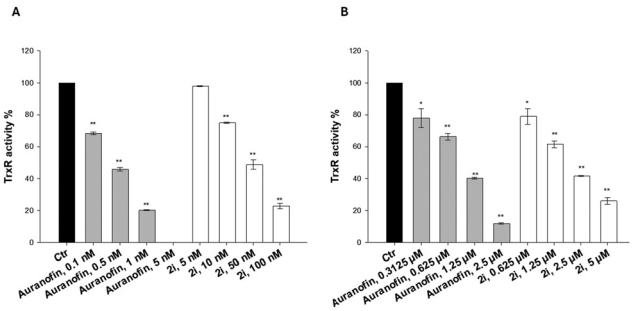

Fig. 5 TrxR inhibition. (A) TrxR1 activity was assayed by measuring the NADPH-dependent reduction of DTNB at 412 nm as described in the Experimental section. Error bars indicate S.D. (B) A2780 cells were incubated for 24 h with **2i** or auranofin. Subsequently, TrxR activity was tested in cell lysates by measuring the NADPH-dependent reduction of DTNB at 412 nm. Error bars indicate SD. * $p < 0.05$; ** $p < 0.01$.

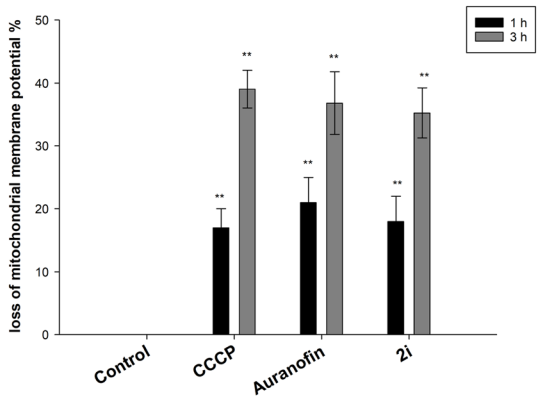

Fig. 6 A2780 cells were treated for 3 or 6 h with IC_{50} concentrations of the tested complexes or CCCP (3 μM). The percentage of depleted mitochondrial membrane potential was determined by the MITO-ID® membrane potential kit. Results are the means of three independent experiments. Error bars indicate S.D. *$p < 0.05$, **$p < 0.01$.

mitochondrial function and inducing cell death, primarily through the induction of severe oxidative stress and the consequent loss of mitochondrial membrane potential ($\Delta\Psi_m$). On this basis, we evaluated the ability of compound **2i** to induce mitochondrial membrane potential depletion in ovarian cancer cells.

A2780 cells were treated with **2i** or auranofin for 1 or 3 h, and the percentage of cells with depolarized mitochondrial membrane potential was determined by means of the MITO-ID® membrane potential kit. Carbonyl cyanide m-chlorophenyl hydrazone (CCCP) was used as a positive control. The results depicted in Fig. 6 show that the percentage mitochondrial membrane potential loss was time dependent for all the tested compounds.

Conclusions

In this study, we developed a robust and general synthetic strategy for the preparation of heterobimetallic Pd(II)/Sn(II) η^3-

allyl complexes bearing N-heterocyclic carbene ligands, thereby expanding the chemical space of biologically active palladium- and tin-based organometallics. The straightforward insertion of $SnCl_2$ into the Pd–Cl bond of the corresponding allyl–palladium precursors proceeds smoothly under mild conditions, providing a library of thirteen well-defined complexes. Full spectroscopic characterization, complemented by single-crystal X-ray diffraction where applicable, unequivocally confirmed their molecular structures, while DFT calculations elucidated the underlying reaction mechanism, revealing a single-step process driven by a favourable Cl···$SnCl_2$ interaction, culminating in insertion of $SnCl_2$ into the Pd–Cl bond. Beyond their synthetic significance, these heterobimetallic complexes display a striking and coherent biological profile. Across a comprehensive panel of ovarian cancer cell lines—including cisplatin-sensitive, cisplatin-resistant, and high-grade serous ovarian cancer (HGSOC) models—all compounds demonstrated substantial antiproliferative activity, with selected derivatives combining high potency and pronounced tumour selectivity. Among them, compound **2i** clearly stands out, displaying cytotoxic activity that is generally superior to that of cisplatin while achieving an approximately two orders of magnitude higher selectivity towards tumour cells. Notably, comparison with the corresponding precursor complex bearing a chloride ligand in place of the trichlorostannyl fragment indicates that, in the case of the lead compound **2i**, the incorporation of the $SnCl_3$ ligand results in a marked increase in *in vitro* tumour selectivity over normal cells, highlighting the beneficial contribution of the $SnCl_3$ fragment to the biological profile of these complexes.

Importantly, the therapeutic potential of compound **2i** extends well beyond conventional 2D cell culture models. Its potent antitumour activity is fully retained in patient-derived tumour organoids (PDTOs) established from HGSOC samples, including models resistant to platinum-based chemotherapy, thereby underscoring the translational relevance of this compound. At the same time, **2i** shows no detectable toxicity towards non-cancerous fallopian tube epithelium organoids, highlighting a favourable therapeutic window and validating the predictive power of organoid-based platforms in discriminating efficacy from off-target toxicity.

Mechanistic investigations further reveal that compound **2i** operates through a mode of action fundamentally distinct from that of classical platinum-based drugs. Specifically, **2i** effectively inhibited TrxR activity, thereby inducing a loss of mitochondrial membrane potential and rapid cytochrome c release, followed by delayed DNA damage. Notably, the inhibition of TrxR observed for these Pd(II)/Sn(II) heterobimetallic complexes is significantly stronger—both in isolated enzyme and in cellular assays—than that previously measured for the related [Pd(NHC)Cl(allyl)] complexes explored by our group. Moreover, their inhibitory efficiency surpasses that of auranofin, a well-known and potent TrxR inhibitor whose anticancer activity is primarily attributed to this mechanism.

These findings indicate that TrxR inhibition and the consequent mitochondrial dysfunction constitute the primary cytotoxic events triggered by this heterobimetallic complex. While further studies will be required to fully elucidate the specific role of the $SnCl_3$ fragment at the molecular level, the enhanced selectivity and markedly increased TrxR inhibition observed for these heterobimetallic systems suggest that the incorporation of the $SnCl_3$ moiety plays a key role in modulating their biological activity. This mitochondria-centred mechanism provides a compelling explanation for the ability of compound **2i** to overcome platinum-associated resistance mechanisms and positions these organometallic compounds as a mechanistically novel class of metal-based anticancer agents.

Further studies on the detailed mechanism of action and *in vivo* anticancer activity of these compounds are currently underway in our laboratories, paving the way toward their potential translation into next-generation metal-based chemotherapeutics.

Experimental section

All the complexes synthesised in this study, with the only exception of complexes **1a–1g**, were prepared under an argon atmosphere using anhydrous dichloromethane, and precipitated from the reaction mixture using anhydrous diethyl-ether and/or *n*-pentane (dried on 4 Å molecular sieves according to literature[91]). For complexes **1a–1g**, technical grade acetone was used, with no need for an inert atmosphere.

The NMR characterization was possible using the Bruker Avance 300 and Bruker Avance 400 spectrometer at room temperature. For complex **2m**, ^{1}H NMR, ^{13}C{^{1}H} NMR and the bidimensional HMQC and HMBC spectra were registered at 253 K to distinguish two different isomers. In the case of compound **2c**, only the ^{1}H NMR spectra were registered at 223 K, to better resolve the different peaks. Anhydrous $CDCl_3$ and CD_2Cl_2 (dried on 4 Å molecular sieves) were used as solvents.

The IR spectra were recorded in KBr tablets using the PerkinElmer Spectrum One spectrophotometer. Elemental analyses were carried out using an Elemental CHN "CUBO Micro Vario" analyser.

X-ray crystallographic structures were collected at 100 K, 200 K or 298 K at the XRD2 beamline of the Elettra Synchrotron, Trieste (Italy), using a monochromatic wavelength.

Synthesis of complexes 1a–1m

The palladium(II)–allyl precursors **1a–1m** were prepared according to known synthetic procedures. Particularly, for compound **1a–g**, the weak-base route was used.[68,69,92] Briefly, a stoichiometric amount of the respective imidazolium salt was added to a solution of $[Pd(allyl)Cl]_2$ (or $[Pd(2\text{-methyl-allyl})Cl]_2$, $[Pd(1,1\text{-dimethyl-allyl})Cl]_2$) in technical grade acetone. Then, an excess (~3 equiv.) of K_2CO_3 was added, and the reaction was stirred for 5 h. The desired complexes were obtained by simple filtration and solvent removal at reduced pressure. All these complexes have already been reported and exhaustively characterized in the literature.

In contrast, for compounds **1h–m** the transmetalation route was employed.[78,79] At first, the [Ag(NHC)Cl] precursors were prepared using a well-established procedure[78,79,93,94] which consisted of the reaction between Ag_2O (0.6 equiv.) and the respective azolium salt under an argon atmosphere and using dichloromethane as solvent. The reaction mixture was stirred for 24 hours in the dark, to avoid light degradation. The final suspension was filtered on a Millipore filter, the solvent was subsequently reduced under vacuum, and the final products were finally obtained as powder and filtered on a Gooch filter after precipitation with Et_2O. For the complex bearing Me-Im-^{t}Bu as the ancillary ligand, whose synthesis is not described in literature with chloride as the counterion of the imidazolium salt, the synthetic procedure is reported in detail in this Experimental section.

After obtaining the silver–carbene complexes, they were reacted with a stoichiometric amount of $[Pd(allyl)Cl]_2$ (or the substituted $[Pd(2\text{-methyl-allyl})Cl]_2$) previously dissolved in anhydrous dichloromethane. The reaction mixture was stirred for 45 minutes under an argon atmosphere and in the dark. After the indicated time, suspension was centrifuged at 5000 rpm for 10 minutes, thus precipitating AgCl (obtained as byproduct), and the supernatant was filtered using a Millipore filter. The solvent of the obtained solution was reduced under vacuum and the final complexes precipitated after the addition of a mixture of Et_2O and *n*-pentane. All complexes have already been reported in the literature, with the exception of complexes **1h**, **1j** and **1k**, whose synthetic procedure is reported in detail below.

Synthesis of [Ag(Me-Im-^{t}Bu)Cl]

150 mg (0.859 mmol) of the imidazolium salt [Me-Im-^{t}Bu]·HCl were dissolved in 20 mL of CH_2Cl_2 and reacted with 119.6 mg (0.516 mmol) of Ag_2O using the above-described conditions. 174 mg of the desired product was obtained (yield 72%). ^{1}H NMR (300 MHz, $CDCl_3$, T = 298 K, ppm) δ: 7.15 (d, J = 1.9 Hz, 1H, CH^{Im}), 6.93 (d, J = 1.9 Hz, 1H, CH^{Im}), 3.87 (s, 3H, N-CH_3), 1.71 (s, 9H, ^{t}Bu-CH_3). $^{13}C\{^1H\}$ NMR (76 MHz, $CDCl_3$, T = 298 K, ppm) δ: 178.7 (C, $C^{carbene}$, detected by HMBC), 120.6 (CH, CH^{Im}), 119.0 (CH, CH^{Im}), 58.0 (C, ^{t}Bu-C), 40.0 (CH_3, N-CH_3), 32.0 (CH_3, ^{t}Bu-CH_3).

Synthesis of [Pd(Tol-CH_2-Im-CH_2-Tol)(allyl)Cl] (1h). The compound was obtained using the abovementioned procedure, using 70.0 mg (0.191 mmol) of $[Pd(allyl)Cl]_2$ and 160.4 mg (0.383 mmol) of the corresponding silver–carbene precursor in 15 mL of anhydrous CH_2Cl_2. 155.0 mg of the desired complex was obtained (yield 86%). ^{1}H NMR (300 MHz, $CDCl_3$, T = 298 K, ppm) δ: 7.15 (d, J = 1.2 Hz, 8H, aryl-H), 6.84 (s, 2H, CH^{Im}), 5.53–5.29 (m, 4H, CH_2-N), 5.23–5.07 (m, 1H, H^2), 4.25 (dd, J = 7.6, 2.2 Hz, 1H, *syn*-H^1), 3.19 (d, J = 13.6 Hz, 1H, *anti*-H^1), 3.12 (d, J = 6.6 Hz, 1H, *syn*-H^3), 2.33 (s, 6H, Tol-CH_3), 2.02 (d, J = 11.8 Hz, 1H, *anti*-H^3). $^{13}C\{^1H\}$ NMR (76 MHz, $CDCl_3$, T = 298 K, ppm) δ: 181.2 (C, $C^{carbene}$), 138.1 (C, *p*-aryl-C), 133.6 (C, *ipso*-aryl-C), 129.6 (CH, *m*-aryl-CH), 128.1 (CH, *o*-aryl-CH), 121.5 (CH, CH^{Im}), 115.0 (CH, C^2), 73.0 (CH_2, C^1), 54.8 (CH_2, N-CH_2), 48.7 (CH_2, C^3), 21.3 (CH_3, Tol-CH_3).

Synthesis of [Pd(Me-Im-Mes)(2-methyl-allyl)Cl] (1j). The compound was obtained using the abovementioned procedure, using 70.0 mg (0.177 mmol) of $[Pd(2\text{-methyl-allyl})Cl]_2$ and 122.1 mg (0.355) mmol of the corresponding silver–carbene precursor in 15 mL of anhydrous CH_2Cl_2. 118.7 mg of the desired complex was obtained (yield 84%). ^{1}H NMR (300 MHz, $CDCl_3$, T = 298 K, ppm) δ: 7.08 (d, J = 1.8 Hz, 1H, CH^{Im}), 6.94 (s, 1H, *m*-aryl-H), 6.91 (s, 1H, *m*-aryl-H), 6.87 (d, J = 1.8 Hz, 1H, CH^{Im}), 4.07 (s, 3H, N-CH_3), 3.85 (d, J = 3.1 Hz, 1H, *syn*-H^1), 2.89 (s, 1H, *anti*-H^1), 2.81 (d, J = 3.2 Hz, 1H, *syn*-H^3), 2.30 (s, 3H, *p*-Mes-CH_3), 2.11 (s, 3H, *o*-Mes-CH_3), 2.09 (s, 3H, *o*-Mes-CH_3), 1.89 (s, 1H, *anti*-H^3), 1.44 (s, 3H, allyl-CH_3). $^{13}C\{^1H\}$ NMR (76 MHz, $CDCl_3$, T = 298 K, ppm) δ: 182.9 (C, $C^{carbene}$), 138.9 (C, *p*-aryl-C), 136.7 (C, *o*-aryl-C), 136.2 (C, *o*-aryl-C), 135.4 (C, *ipso*-aryl-C), 129.3 (C, C^2), 129.1 (CH, *m*-aryl-CH), 128.9 (CH, *m*-aryl-CH), 122.6 (CH, CH^{Im}), 122.2 (CH, CH^{Im}), 70.8 (CH_2, C^1), 49.1 (CH_2, C^3), 38.6 (CH_3, N-CH_3), 22.8 (CH_3, allyl-CH_3), 21.1 (CH_3, *p*-Mes-CH_3), 18.4 (CH_3, *o*-Mes-CH_3), 18.3 (CH_3, *o*-Mes-CH_3).

Synthesis of [Pd(Me-Im-^{t}Bu)(allyl)Cl] (1k). The compound was obtained using the abovementioned procedure, using 70.0 mg (0.191 mmol) of $[Pd(allyl)Cl]_2$ and 107.7 mg (0.383 mmol) of the corresponding silver–carbene precursor in 15 mL of anhydrous CH_2Cl_2. 116.2 mg of the desired complex was obtained (yield 95%). ^{1}H NMR (300 MHz, $CDCl_3$, T = 298 K, ppm) δ: more abundant isomer (~57%): 7.09 (d, J = 2.0 Hz, 1H, CH^{Im}), 6.91 (d, J = 2.0 Hz, 1H, CH^{Im}), 5.33–5.18 (m, 1H, H^2), 4.26–4.19 (m, 1H, *syn*-H^1), 4.03 (s, 3H, N-CH_3), 3.33–3.23 (m, 2H, *syn*-H^3, *anti*-H^1), 2.49 (d, J = 11.9 Hz, 1H, *anti*-H^3), 1.68 (s, 9H, ^{t}Bu-CH_3); less abundant isomer (~43%): 7.11 (d, J = 2.0 Hz, 1H, CH^{Im}), 6.87 (d, J = 2.0 Hz, 1H, CH^{Im}), 5.49–5.30 (m, 1H, H^2), 4.26–4.19 (m, 1H, *syn*-H^1), 3.78 (s, 3H, N-CH_3), 3.48 (m, 1H, *syn*-H^3), 3.33–3.23 (m, 1 H, *anti*-H^1), 2.27 (d, J = 11.8 Hz, 1H, *anti*-H^3), 1.83 (s, 9H, ^{t}Bu-CH_3). $^{13}C\{^1H\}$ NMR (76 MHz, $CDCl_3$, T = 298 K, ppm) δ: more abundant isomer (~57%): 179.2 (C, C^{NHC}), 121.0 (CH, CH^{Im}), 119.1 (CH, CH^{Im}), 113.5 (CH, C^2), 71.3 (CH_2, C^1), 58.1 (C, ^{t}Bu-C), 49.5 (CH_2, C^3), 39.5 (CH_3, N-CH_3), 31.6 (CH_3, ^{t}Bu-CH_3); less abundant isomer (~43%): 178.8 (C, $C^{carbene}$), 121.3 (CH, CH^{Im}), 119.0 (CH, CH^{Im}), 113.8 (CH, C^2), 71.3 (CH_2, C^1), 58.1 (C, ^{t}Bu-C), 49.4 (CH_2, C^3), 39.3 (CH_3, N-CH_3), 31.8 (CH_3, ^{t}Bu-CH_3).

Synthesis of complexes 2a–2m

The target complexes were obtained using the same general procedure. A solution in anhydrous dichloromethane of the monometallic [Pd(NHC)Cl(R-allyl)] precursor (**1a–1m**) was prepared in a 100 mL round bottom Schlenk flask, using anhydrous dichloromethane as solvent and under an argon atmosphere. Afterwards, 1.1 equivalents of $SnCl_2$ were added, and the reaction mixture was vigorously stirred for 4 hours at room temperature. Subsequently, the excess of $SnCl_2$ was removed by filtration on a Millipore filter and the obtained solution was dried under vacuum. The final complex was obtained as a microcrystalline powder after the addition of Et_2O/*n*-pentane and finally filtered on a sintered glass filter.

Synthesis of [Pd(IMes)(allyl)SnCl$_3$] (2a). The compound was synthesised according to the abovementioned general procedure. Specifically, 80.5 mg (0.164 mmol) of **1a** were reacted with 31.2 mg (0.165 mmol) of $SnCl_2$. 82.1 mg of the desired product was obtained (yield 74%). ^{1}H NMR (300 MHz, CD_2Cl_2, T = 253 K, ppm) δ: 7.28 (s, 2H, CH^{Im}), 6.98 (d, J = 10.8 Hz, 4H, *m*-aryl-H), 4.89–4.70 (m, 1H, H^2), 4.35 (d, J = 7.0 Hz, 1H, *syn*-H^3), 4.18 (d, J = 7.5 Hz, 1H, *syn*-H^1), 2.43 (d, J = 14.7 Hz, 1H, *anti*-H^3), 2.32 (d, J = 6.1 Hz, 1H, *anti*-H^1), 2.29 (s, 6H, *p*-Mes-CH_3), 2.16 (s, 6H, *o*-Mes-CH_3), 2.14 (s, 6H, *o*-Mes-CH_3). $^{13}C\{^1H\}$ NMR (76 MHz, $CDCl_3$, T = 298 K, ppm) δ: 180.3 (C, $C^{carbene}$) 139.8 (C, *p*-aryl-C), 135.2 (C, *ipso*-aryl-C), 134.8 (C, aryl-C), 134.5 (C, aryl-C), 129.9 (CH, *m*-aryl-CH), 129.8 (CH, *m*-aryl-CH), 124.2 (CH, CH^{Im}), 116.5 (CH, C^2), 69.5 (C H_2, C^3), 63.7 (CH_2, C^1), 21.2 (CH_3, *p*-Mes-CH_3), 18.6 (CH_3, *o*-Mes-CH_3). IR (KBr pellet): ν_{Sn-Cl} = 312, 336 cm^{-1}. Elemental analysis calcd (%) for $C_{24}H_{29}Cl_3N_2PdSn$: C, 42.58; H, 4.32; N, 4.14. Found: C, 42.35; H, 4.40; N, 4.26.

Synthesis of [Pd(IMes)(2-methyl-allyl)SnCl$_3$] (2b). The compound was synthesised according to the abovementioned general procedure. Specifically, 80.0 mg (0.159 mmol) of **1b** were reacted with 33.3 mg (0.175 mmol) of $SnCl_2$. 101.4 mg of the desired product was obtained (yield 92%). ^{1}H NMR (300 MHz, CD_2Cl_2, T = 298 K, ppm) δ: 7.27 (s, 2H, CH^{Im}), 7.02 (d, J = 7.5 Hz, 4H, *m*-aryl-H), 4.03 (d, J = 4.5 Hz, 2H, *syn*-H^1, *syn*-H^3), 2.56 (s, 1H, *anti*-H^3), 2.32 (s, 6H, *p*-Mes-CH_3), 2.25 (s, 1H, *anti*-H^1), 2.18 (s, 6H, *o*-Mes-CH_3), 2.13 (s, 6H, *o*-Mes-CH_3), 1.20 (s, 3H, allyl-CH_3). $^{13}C\{^1H\}$ NMR (76 MHz, $CDCl_3$, T = 298 K, ppm) δ: 181.3 (C, C^{NHC}), 139.8 (C, *p*-aryl-C), 135.4 (C, *ipso*-aryl-C), 134.8 (C, *o*-aryl-C), 134.6 (C, *o*-aryl-C), 131.3 (C, C^2), 129.9 (CH, *m*-aryl-CH), 124.2 (CH, CH^{Im}), 68.5 (CH_2, C^3), 64.1 (CH_2, C^1), 22.5 (CH_3, allyl-CH_3), 21.2 (CH_3, *p*-Mes-CH_3), 18.8 (CH_3, *o*-Mes-CH_3), 18.6 (CH_3, *o*-Mes-CH_3). IR (KBr pellet): ν_{Sn-Cl} = 324, 302 cm^{-1}. Elemental analysis calcd (%) for $C_{25}H_{31}Cl_3N_2PdSn$: C, 43.45; H, 4.52; N, 4.05. Found: C, 43.10; H, 4.67; N, 3.97.

Synthesis of [Pd (IMes)(1,1-dimethyl-allyl)SnCl$_3$] (2c). The compound was synthesised according to the abovementioned general procedure. Specifically, 80.0 mg (0.155 mmol) of **1c** were reacted with 32.8 mg (0.171 mmol) of $SnCl_2$. 92.9 mg of the desired product was obtained (yield 85%). ^{1}H NMR (300 MHz, CD_2Cl_2, T = 223 K, ppm) δ: 7.31 (d, J = 1.9 Hz, 1H, CH^{Im}), 7.26 (d, J = 1.9 Hz, 1H, CH^{Im}), 7.01 (s, 1H, *m*-aryl-H), 7.01 (s, 1H, *m*-aryl-H), 6.98 (s, 1H, *m*-aryl-H), 6.93 (s, 1H, *m*-aryl-H), 4.62 (dd, J = 13.4, 7.6 Hz, 1H, H^2), 3.75 (dd, J = 7.6, 1.8 Hz, 1H, *syn*-H^3), 2.29 (s, 3H, Mes-CH_3), 2.26 (s, 3H, Mes-CH_3), 2.21 (s, 4H, Mes-CH_3, *anti*-H^3), 2.18 (s, 3H, Mes-CH_3), 2.06 (s, 3H, Mes-CH_3), 1.98 (s, 3H, Mes-CH_3), 1.88 (s, 3H, *syn*-allyl-CH_3), 0.74 (s, 3H, *anti*-allyl-CH_3). $^{13}C\{^1H\}$ NMR (76 MHz, $CDCl_3$, T = 298 K, ppm) δ: 139.6 (C, *p*-aryl-C), 134.9 (C, *o*-aryl-C), 129.6 (CH, *m*-aryl-CH), 124.0 (CH, CH^{Im}), 66.0 (CH_2, allyl C^3), 21.2 (CH_3, Mes-CH_3), 19.9 (CH_3, *anti*-allyl-CH_3), 18.9 (CH_3, Mes-CH_3). C^1 and C^3 non-detected. IR (KBr pellet): ν_{Sn-Cl} = 326, 303 cm^{-1}. Elemental analysis calcd (%) for $C_{26}H_{33}Cl_3N_2PdSn$: C, 44.29; H, 4.72; N, 3.97. Found: C, 43.92; H, 4.81; N, 4.06.

Synthesis of [Pd(IPr)(allyl)SnCl$_3$] (2d). The compound was synthesised according to the abovementioned general procedure. Specifically, 80.0 mg (0.140 mmol) of **1d** were reacted with 29.2 mg (0.154 mmol) of $SnCl_2$. 86.0 mg of the desired product was obtained (yield 81%). ^{1}H NMR (300 MHz, CD_2Cl_2, T = 298 K, ppm) δ: 7.47 (t, J = 7.8 Hz, 2H, *p*-aryl-H), 7.37 (s, 2H, CH^{Im}), 7.35 (d, J = 1.6 Hz, 1H, *m*-aryl-H), 7.33 (d, J = 1.6 Hz, 1H, *m*-aryl-H), 7.32 (d, J = 7.8 Hz, 1H, *m*-aryl-H), 7.29 (d, J = 7.8 Hz, 1H, *m*-aryl-H), 4.87–4.67 (m, 1H, H^2), 4.79 (bs, 1H, *syn*-H^3), 4.21 (d, J = 7.5 Hz, 1H, *syn*-H^1), 3.00 (hept, J = 6.8 Hz, 2H, iPr-CH), 2.79 (hept, J = 6.8 Hz, 2H, iPr-CH), 2.38 (d, J = 13.4 Hz, 1H, *anti*-H^3), 2.22 (d, J = 13.2 Hz, 1H, *anti*-H^1), 1.41 (d, J = 6.8 Hz, 6H, iPr-CH_3), 1.32 (d, J = 6.8 Hz, 6H, iPr-CH_3), 1.20 (d, J = 6.8 Hz, 6H, iPr-CH_3), 1.09 (d, J = 6.8 Hz, 6H, iPr-CH_3). $^{13}C\{^1H\}$ NMR (76 MHz, $CDCl_3$, T = 298 K, ppm) δ: 183.5 (C, $C^{carbene}$, detected by HMBC), 145.9 (C, *o*-aryl-C), 145.6 (C, *o*-aryl-C), 135.2 (C, *ipso*-aryl-C), 130.7 (CH, *p*-aryl-CH), 125.6 (CH, CH^{Im}), 124.7 (CH, *m*-aryl-CH), 124.5 (CH, *m*-aryl-CH), 116.2 (CH, C^2), 70.1 (CH_2, C^3), 63.2 (CH_2, C^1), 28.9 (CH, iPr-CH), 28.7 (CH, iPr-CH), 27.0 (CH_3, iPr-CH_3), 26.1 (CH_3, iPr-CH_3), 23.4 (CH_3, iPr-CH_3), 23.0 (CH_3, iPr-CH_3). IR (KBr pellet): ν_{Sn-Cl} = 332, 307 cm^{-1}. Elemental analysis calcd (%) for $C_{30}H_{41}Cl_3N_2PdSn$: C, 47.34; H, 5.43; N, 3.68. Found: C, 47.60; H, 5.28; N, 3.59.

Synthesis of [Pd(IPr)(2-methyl-allyl)SnCl$_3$] (2e). The compound was synthesised according to the abovementioned general procedure. Specifically, 80.0 mg (0.136 mmol) of **1e** were reacted with 28.5 mg (0.150 mmol) of $SnCl_2$. 89.3 mg of the desired product was obtained (yield 84%). ^{1}H NMR (300 MHz, CD_2Cl_2, T = 253 K, ppm) δ: 7.47 (t, J = 7.7 Hz, 2H, *p*-aryl-H), 7.37 (s, 3H, CH^{Im}; *m*-aryl-H), 7.34 (d, J = 1.5 Hz, 1H, *m*-aryl-H), 7.29 (d, J = 1.5 Hz, 1H, *m*-aryl-H), 7.26 (d, J = 1.5 Hz, 1H, *m*-aryl-H), 4.07 (d, J = 3.3 Hz, 1H, *syn*-H^1), 3.93 (d, J = 3.3 Hz, 1H, *syn*-H^3), 2.90 (hept, J = 6.9 Hz, 2H, iPr-CH), 2.70 (hept, J = 6.9 Hz, 2H, iPr-CH), 2.58 (s, 1H, *anti*-H^3), 2.25 (s, 1H, *anti*-H^1), 1.43 (d, J = 6.8 Hz, 6H, iPr-CH_3), 1.24 (d, J = 6.9 Hz, 6H, iPr-CH_3), 1.19 (d, J = 6.7 Hz, 6H, iPr-CH_3) 1.02 (d, J = 6.8 Hz, 6H, iPr-CH_3), 0.95 (s, 3H, allyl-CH_3). $^{13}C\{^1H\}$ NMR (76 MHz, $CDCl_3$, T = 298 K, ppm) δ: 184.5 (C, $C^{carbene}$), 145.9 (C, *o*-aryl-C), 145.6 (C, *o*-aryl-C), 135.6 (C, *ipso*-aryl-C), 131.5 (C, C^2), 130.6 (CH, *p*-aryl-C), 125.6 (CH, CH^{Im}), 124.7 (CH, *m*-aryl CH), 124.5 (CH, *m*-aryl CH), 67.8 (CH_2, C^3), 65.3 (CH_2, C^1), 28.8 (CH, iPr-CH), 28.7 (CH, iPr-CH), 27.0 (CH_3, iPr-CH_3), 26.1 (CH_3, iPr-CH_3), 23.4 (CH_3, iPr-CH_3), 22.9 (CH_3, iPr-CH_3), 22.6 (CH_3, allyl-CH_3). IR (KBr pellet): ν_{Sn-Cl} = 326, 304 cm^{-1}. Elemental analysis calcd (%) for $C_{31}H_{43}Cl_3N_2PdSn$: C, 48.03; H, 5.59; N, 3.61. Found: C, 48.36; H, 5.43; N, 3.54.

Synthesis of [Pd(SIMes)(allyl)SnCl$_3$] (2f). The compound was synthesised according to the abovementioned general procedure. Specifically, 70.0 mg (0.143 mmol) of **1f** were reacted with 29.8 mg (0.157 mmol) of $SnCl_2$. 89.0 mg of the desired product was obtained (yield 92%). ^{1}H NMR (300 MHz, CD_2Cl_2, T = 298 K, ppm) δ: 6.95 (d, J = 9.0 Hz, 4H, *m*-aryl-H), 4.84–4.60 (m, 1H, H^2), 4.46 (d, J = 7.2 Hz, 1H, *syn*-H^3), 4.13 (d, J = 7.9 Hz, 1H, *syn*-H^1), 4.07 (m, 4H, CH_2^{Im}), 2.46 (d, J = 13.4 Hz, 1H, *anti*-H^3), 2.41 (s, 6H, *o*-Mes-CH_3), 2.34 (s, 6H, *o*-Mes-CH_3), 2.27 (s, 6H, *p*-Mes-CH_3), 2.22 (d, J = 12.7 Hz, 1H, *anti*-H^1). $^{13}C\{^1H\}$

NMR (76 MHz, $CDCl_3$, T = 298 K, ppm) δ: 209.7 ($C^{carbene}$), 139.0 (C, *p*-aryl-C), 135.6 (C, *ipso*-aryl-C), 135.5 (C, *o*-aryl-C), 135.0 (C, *o*-aryl-C), 130.1 (CH, *m*-aryl-CH), 130.0 (CH, *m*-aryl-CH), 116.6 (CH, C^2), 69.6 (CH_2, C^3), 63.9 (CH_2, C^1), 51.9 (CH_2, CH_2^{Im}), 21.2 (CH_3, *p*-Mes-CH_3), 18.7 (CH_3, *o*-Mes-CH_3), 18.7 (*o*-Mes-CH_3). IR (KBr pellet): ν_{Sn-Cl} = 326, 307 cm^{-1}. Elemental analysis calcd (%) for $C_{24}H_{31}Cl_3N_2PdSn$: C, 42.45; H, 4.60; N, 4.13. Found: C, 42.08; H, 4.70; N, 4.25.

Synthesis of [Pd(SIPr)(allyl)$SnCl_3$] (2g). The compound was synthesised according to the abovementioned general procedure. Specifically, 80.0 mg (0.139 mmol) of **1g** were reacted with 29.1 mg (0.153 mmol) of $SnCl_2$. 87.6 mg of the desired product was obtained (yield 82%). ^{1}H NMR (300 MHz, CD_2Cl_2, T = 253 K, ppm) δ: 7.36 (t, J = 7.7 Hz, 2H, *p*-aryl-H), 7.28 (d, J = 1.7 Hz, 1H, *m*-aryl-H), 7.26 (d, J = 1.7 Hz, 1H, *m*-aryl-H), 7.21 (d, J = 1.7 Hz, 1H, *m*-aryl-H), 7.18 (d, J = 1.7 Hz, 1H, *m*-aryl-H), 4.79–4.60 (m, 1H, H^2), 4.26–4.03 (m, 6H, *syn*-H^3; *syn*-H^1; CH_2^{Im}), 3.38–3.17 (m, 4H, iPr CH), 2.08 (d, J = 13.4 Hz, 1H, *anti*-H^3), 1.93 (d, J = 13.5 Hz, 1H, *anti*-H^1), 1.45 (d, J = 6.7 Hz, 6H, iPr-CH_3), 1.27 (d, J = 6.8 Hz, 6H, iPr-CH_3), 1.23 (d, J = 6.9 Hz, 6H, iPr-CH_3), 1.18 (d, J = 6.8 Hz, 6H, iPr-CH_3). $^{13}C\{^1H\}$ NMR (76 MHz, $CDCl_3$, T = 298 K, ppm) δ: 212.3 (C, $C^{carbene}$), 147.1 (C, *o*-aryl-C), 146.7 (C, *o*-aryl-C), 135.6 (C, *ipso*-aryl-C), 129.8 (CH, *p*-aryl-CH), 124.9 (CH, *m*-aryl-CH), 124.8 (CH, *m*-aryl-CH), 116.3 (CH, C^2), 70.3 (CH_2, C^3), 63.3 (CH_2, C^1), 54.5 (CH_2, CH_2^{Im}), 28.9 (CH, iPr-CH), 28.7 (CH, iPr-CH), 27.4 (CH_3, iPr-CH_3), 27.0 (CH_3, iPr-CH_3), 24.1 (CH_3, iPr-CH_3), 24.0 (CH_3, iPr-CH_3). IR (KBr pellet): ν_{Sn-Cl} = 329, 305 cm^{-1}. Elemental analysis calcd (%) for $C_{30}H_{43}Cl_3N_2PdSn$: C, 47.22; H, 5.68; N, 3.67. Found: C, 47.06; H, 5.80; N, 3.75.

Synthesis of [Pd(Tol-CH_2-Im-CH_2-Tol)(allyl)$SnCl_3$] (2h). The compound was synthesised according to the abovementioned general procedure. Specifically, 80.0 mg (0.174 mmol) of **1h** were reacted with 36.4 mg (0.192 mmol) of $SnCl_2$. 101.7 mg of the desired product was obtained (yield 90%). ^{1}H NMR (300 MHz, CD_2Cl_2, T = 253 K, ppm) δ: 7.20–7.05 (m, 8H, aryl-CH), 6.99 (d, J = 7.8 Hz, 2H, CH^{Im}), 5.18, 5.11 (AB system, J = 15.0 Hz, 2H, N-CH_2), 5.00, 4.90 (AB system, J = 15.0 Hz, 2H, N-CH_2), 4.79–4.62 (m, 1H, H^2), 4.32 (d, J = 7.1 Hz, 1H, *syn*-H^1), 3.79 (d, J = 7.4 Hz, 1H, *syn*-H^3), 2.33 (d, J = 7.1 Hz, 1H, *anti*-H^3; partially obscured), 2.30 (s, 3H, Tol-CH_3), 2.27 (s, 3H, Tol-CH_3), 1.96 (d, J = 13.3 Hz, 1H, *anti*-H^1). $^{13}C\{^1H\}$ NMR (76 MHz, $CDCl_3$, T = 298 K, ppm) δ: 176.9 (C, $C^{carbene}$; detected by HMBC), 138.7 (C, *p*-aryl-C), 132.7 (CH, *ipso*-aryl-CH), 129.8 (CH, *m*-aryl-CH), 128.1 (CH, *o*-aryl-CH), 123.0 (CH, CH^{Im}), 117.1 (CH, C^2), 67.5 (CH_2, C^3), 62.1 (CH_2, C^1), 55.3 (CH_2, CH_2-N), 21.3 (CH_3, Tol-CH_3). IR (KBr pellet): ν_{Sn-Cl} = 333, 309 cm^{-1}. Elemental analysis calcd (%) for $C_{22}H_{25}Cl_3N_2PdSn$: C, 40.72; H, 3.88; N, 4.32. Found: C, 40.38; H, 3.95; N, 4.39.

Synthesis of [Pd(Me-Im-Mes)(allyl)$SnCl_3$] (2i). The compound was synthesised according to the abovementioned general procedure. Specifically, 80.0 mg (0.208 mmol) of **1i** were reacted with 43.3 mg (0.218 mmol) of $SnCl_2$. 105.3 mg of the desired product was obtained (yield 89%). ^{1}H NMR (300 MHz, CD_2Cl_2, T = 253 K, ppm) δ: 7.27 (d, J = 1.9 Hz, 1H, CH^{Im}), 7.09 (d, J = 1.9 Hz, 1H, CH^{Im}), 6.93 (d, J = 4.5 Hz, 2H, *m*-aryl-H), 5.02–4.85 (m, 1H, H^2), 4.35 (d, J = 6.9 Hz, 2H, *syn*-H^3; *syn*-H^1), 3.79 (s, 3H, N-CH_3), 2.58 (d, J = 13.5 Hz, 1H, *anti*-H^3), 2.45 (dd, J = 13.3, 1.1 Hz, 1H, *anti*-H^1), 2.27 (s, 3H, Mes-CH_3), 2.05 (s, 3H, Mes-CH_3), 1.97 (s, 3H, Mes-CH_3). $^{13}C\{^1H\}$ NMR (76 MHz, $CDCl_3$, T = 298 K, ppm) δ: 177.8 (C, $C^{carbene}$), 139.5 (C, *p*-aryl C), 135.5 (C, *o*-aryl C), 135.1 (C, *o*-aryl C), 129.5 (CH, *m*-aryl-CH), 129.2 (CH, *m*-aryl-CH), 124.1 (CH, CH^{Im}), 123.6 (CH^{Im}), 116.8 (CH, C^2), 68.7 (CH_2, C^1), 62.0 (CH_2, C^3), 39.1 (N-CH_3), 21.2 (CH_3, *p*-Mes-CH_3), 18.5 (CH_3, *o*-Mes-CH_3), 18.2 (CH_3, *o*-Mes-CH_3). IR (KBr pellet): ν_{Sn-Cl} = 326, 302 cm^{-1}. Elemental analysis calcd (%) for $C_{16}H_{21}Cl_3N_2PdSn$: C, 33.55; H, 3.70; N, 4.89. Found: C, 33.40; H, 3.79; N, 4.80.

Synthesis of [Pd(Me-Im-Mes)(2-methyl-allyl)$SnCl_3$] (2j). The compound was synthesised according to the abovementioned general procedure. Specifically, 80.0 mg (0.201 mmol) of **1j** were reacted with 42.0 mg (0.221 mmol) of $SnCl_2$. 102.1 mg of the desired product was obtained (yield 86%). ^{1}H NMR (300 MHz, CD_2Cl_2, T = 253 K, ppm) δ: 7.27 (d, J = 1.9 Hz, 1H, CH^{Im}), 7.08 (d, J = 1.9 Hz, 1H, CH^{Im}), 6.96 (s, 1H, *m*-aryl-H), 6.91 (s, 1H, *m*-aryl-H), 4.11 (d, J = 2.5 Hz, 1H, *syn*-H^3), 3.99 (d, J = 3.2 Hz, 1H, *syn*-H^1), 3.84 (s, 3H, N-CH_3), 2.69 (s, 1H, *anti*-H^1), 2.35 (s, 1H, *anti*-H^3), 2.26 (s, 3H, *p*-Mes-CH_3), 2.02 (s, 3H, *o*-Mes-CH_3), 1.96 (s, 3H, *o*-Mes-CH_3), 1.21 (s, 3H, allyl-CH_3). $^{13}C\{^1H\}$ NMR (76 MHz, $CDCl_3$, T = 298 K, ppm) δ: 178.4 (C, $C^{carbene}$), 139.5 (C, *p*-aryl-C), 135.6 (C, *o*-aryl-C), 135.1 (C, *o*-aryl-C), 131.5 (C, C^2), 129.4 (CH, *m*-aryl-CH), 129.3 (CH, *m*-aryl-CH), 124.1 (CH, CH^{Im}), 123.5 (CH, CH^{Im}), 67.8 (CH_2, C^1), 61.8 (CH_2, C^3), 39.2 (CH_3, N-CH_3), 23.1 (CH_3, allyl-CH_3), 21.1 (CH_3, *p*-Mes-CH_3), 18.4 (CH_3 *o*-Mes-CH_3), 18.4 (CH_3 *o*-Mes-CH_3). IR (KBr pellet): ν_{Sn-Cl} = 326, 303 cm^{-1}. Elemental analysis calcd (%) for $C_{17}H_{23}Cl_3N_2PdSn$: C, 34.79; H, 3.95; N, 4.77. Found: C, 35.06; H, 3.82; N, 4.84.

Synthesis of [Pd(Me-Im-^{t}Bu)(allyl)$SnCl_3$] (2k). The compound was synthesised according to the abovementioned general procedure. Specifically, 50.8 mg (0.158 mmol) of **1k** were reacted with 33.0 mg (0.174 mmol) of $SnCl_2$. 56.6 mg of the desired product was obtained (yield 70%). ^{1}H NMR (300 MHz, CD_2Cl_2, T = 298 K, ppm) δ: more abundant isomer (~59%): 7.28 (d, J = 1.9 Hz, 1H, CH^{Im}), 7.09 (dd, J = 5.9, 1.8 Hz, 1H, CH^{Im}), 5.22 (m, 1H, H^2), 4.55–4.36 (m, 2H, *syn*-H^3; *syn*-H^1), 3.77 (s, 3H, N-CH_3), 3.29 (d, J = 13.4 Hz, 1H, *anti*-H^3), 2.85–2.74 (m, 1H, *anti*-H^1), 1.56 (s, 9H, ^{t}Bu-CH_3). Less abundant isomer (~41%): 7.28 (d, J = 1.9 Hz, 1H, CH^{Im}), 7.09 (dd, J = 5.9, 1.8 Hz, 1H, CH^{Im}), 5.22 (m, 1H, H^2), 4.63 (d, J = 7.2 Hz, 1H, *syn*-H^3), 4.55–4.36 (m, 1H, *syn*-H^1), 3.57 (s, 3H, N-CH_3), 3.13 (d, J = 13.2 Hz, 1H, *anti*-H^3), 2.85–2.74 (m, 1H, *anti*-H^1), 1.68 (s, 9H, ^{t}Bu-CH_3). $^{13}C\{^1H\}$ NMR (76 MHz, $CDCl_3$, T = 298 K, ppm) δ: more abundant isomer: 172.9 (C, C^{NHC}), 122.5 (CH, CH^{Im}), 122.5 (CH, CH^{Im}), 116.3 (CH, C^2), 68.1 (CH, C^3), 61.1 (CH, C^1), 58.2 (C, ^{t}Bu-C), 39.9 (CH_3, N-CH_3), 31.4 (CH_3, ^{t}Bu-CH_3). Less abundant isomer: 172.6 (C, C^{NHC}), 122.9 (CH, CH^{Im}), 120.6 (CH, CH^{Im}), 115.8 (CH, C^2), 68.2 (CH, C^3), 61.1 (CH, C^1), 58.2 (C, ^{t}Bu-C), 39.6 (CH_3, N-CH_3), 31.4 (CH_3, ^{t}Bu-CH_3). IR (KBr pellet): ν_{Sn-Cl} = 326, 303 cm^{-1}. Elemental analysis calcd (%) for $C_{11}H_{19}Cl_3N_2PdSn$: C, 25.87; H, 3.75; N, 5.84. Found: C, 25.76; H, 3.82; N, 5.70.

Synthesis of [Pd((1,5-*a*)pyridin-Im-Mes)(allyl)SnCl$_3$] (2l). The compound was synthesised according to the abovementioned general procedure. Specifically, 80.0 mg (0.190 mmol) of **1i** were reacted with 39.8 mg (0.210 mmol) of $SnCl_2$. 108.9 mg of the desired product was obtained (yield 94%). ^{1}H NMR (300 MHz, CD_2Cl_2, T = 253 K, ppm) δ: 8.04 (d, J = 7.3 Hz, 1H, Py-H^5), 7.50–7.44 (m, 2H, Py-H^8; *m*-aryl-H), 7.05–6.94 (m, 3H, Py-H^6; *m*-aryl-H; CH^{Im}), 6.78 (ddd, J = 6.9 Hz, 1H, Py-H^7), 5.11–4.88 (m, 1H, allyl-H^2), 4.42 (d, J = 7.4 Hz, 1H, *syn*-allyl H^3), 4.36 (d, J = 7.6 Hz, 1H, *syn*-allyl H^1), 2.64–2.51 (m, 2H, *anti*-allyl H^1; *anti*-allyl H^3), 2.30 (s, 3H, Mes-CH$_3$), 2.01 (s, 3H, Mes-CH$_3$), 1.94 (s, 3H, Mes-CH$_3$). ^{13}C{^{1}H} NMR (76 MHz, $CDCl_3$, T = 298 K, ppm) δ: 167.8 (C, C^{carbene}; detected by HMBC), 139.7 (C, *p*-Mes-C), 136.0 (C, *ipso*-Mes-C), 135.2 (C, *o*-Mes-C), 134.7 (C, *o*-Mes-C), 132.3 (C, Py-C^9), 129.5 (CH, *m*-Mes-CH), 129.2 (CH, *m*-Mes-CH), 128.3 (CH, Py-C^5), 123.8 (CH, Py-C^6), 117.8 (CH, Py-C^8), 116.9 (CH, allyl-C^2), 114.5 (CH, Py-C^7), 114.0 (CH, Py-C^1), 69.3 (CH$_2$, allyl-C^3), 62.5 (CH$_2$, allyl-C^1), 21.2 (CH$_3$, Mes-CH$_3$), 18.4 (CH$_3$, Mes-CH$_3$), 18.1 (CH$_3$, Mes-CH$_3$). IR (KBr pellet): ν_{Sn-Cl} = 328, 308 cm^{-1}. Elemental analysis calcd (%) for $C_{19}H_{21}Cl_3N_2PdSn$: C, 37.48; H, 3.48; N, 4.60. Found: C, 37.30; H, 3.55; N, 4.71.

Synthesis of [Pd(Me-ImBz-iPr)(allyl)SnCl$_3$] (2m). The compound was synthesised according to the abovementioned general procedure. Specifically, 80.0 mg (0.224 mmol) of **1m** were reacted with 46.7 mg (0.246 mmol) of $SnCl_2$. 109.9 mg of the desired product was obtained (yield 90%). ^{1}H NMR (300 MHz, $CDCl_3$, T = 253 K, ppm) δ (two isomers, 50 : 50 relative abundance): 7.63–7.54 (m, 2H, benzyl-H), 7.47–7.30 (m, 6H, benzyl-H), 5.42–5.26 (m, 2H, H^2), 4.92 (hept, J = 6.9 Hz, 1H, iPr-CH), 4.68 (hept, J = 6.9 Hz, 1H, iPr-CH; partially obscured), 4.66 (d, J = 5.7 Hz, 2H, *syn*-H^3), 4.59 (d, J = 7.4 Hz, 1H, *syn*-H^1), 4.53 (d, J = 7.4 Hz, 1H, *syn*-H^1), 3.92 (s, 3H, N-CH$_3$), 3.74 (s, 3H, N-CH$_3$), 3.25 (t, J = 12.6 Hz, 2H, *anti*-H^3), 2.96 (d, J = 5.9 Hz, 1H, *anti*-H^1), 2.92 (d, J = 5.9 Hz, 1H, *anti*-H^1), 1.76 (d, J = 7.0 Hz, 3H, iPr-CH$_3$), 1.65 (d, J = 7.0 Hz, 3H, iPr-CH$_3$), 1.63 (d, J = 7.0 Hz, 3H, iPr-CH$_3$), 1.56 (d, J = 7.0 Hz, 3H, iPr-CH$_3$). ^{13}C{^{1}H} NMR (76 MHz, $CDCl_3$, T = 253 K, ppm) δ: 184.7 (C, C^{carbene}), 136.5 (C, benzyl-C), 136.3 (C, benzyl-C), 132.9 (C, benzyl-C), 132.6 (C, benzyl-C), 123.4 (CH, benzyl-CH), 123.4 (CH, benzyl-CH), 123.2 (CH, benzyl-CH), 123.4 (CH, benzyl-CH), 117.8 (CH, benzyl-CH), 117.7 (CH, benzyl-CH), 112.3 (CH, benzyl-CH), 112.1 (CH, benzyl-CH), 110.7 (CH, C^2), 67.2 (CH$_2$, C^3), 67.1 (CH$_2$, C^3), 64.2 (CH$_2$, C^1), 64.1 (CH$_2$, C^1), 55.0 (CH, iPr-CH), 54.1 (CH, iPr-CH), 35.6 (CH$_3$, N-CH$_3$), 35.2 (CH$_3$, N-CH$_3$), 21.7 (CH$_3$, iPr-CH$_3$), 21.6 (CH$_3$, iPr-CH$_3$), 21.3 (CH$_3$, iPr-CH$_3$), 21.3 (CH$_3$, iPr-CH$_3$). IR (KBr pellet): ν_{Sn-Cl} = 326, 305 cm^{-1}. Elemental analysis calcd (%) for $C_{14}H_{19}Cl_3N_2PdSn$: C, 30.75; H, 3.50; N, 5.12. Found: C, 30.50; H, 3.61; N, 5.23.

XRD analysis

2b, **2d** and **2f** crystal data were collected in the XRD2 beamline of the Elettra Synchrotron, Trieste (Italy),[95] using a monochromatic wavelength of 0.620 Å, at 100 K, 200 K or 298 K. The data sets were integrated, scaled and corrected for Lorentz, absorption and polarization effects using the XDS package.[96] Data from two random orientations of the same crystals have been merged to obtain complete datasets for the triclinic **2f** crystal form, using CCP4-Aimless code.[97,98] The structures were solved by direct methods using the SHELXT program[99] and refined using full-matrix least-squares implemented in SHELXL-2019/3.[100] Thermal motions for all non-hydrogen atoms have been treated anisotropically. Hydrogens have been included on calculated positions, riding on their carrier atoms. Geometric restraints (SAME, SADI) have been applied to disordered fragments (allyl ligands and solvent in **2d**). The Coot program was used for structure building.[101] The crystal data are given in Table S1. Pictures were prepared using Ortep-3 [102] and PyMOL[103] software. Crystallographic data have been deposited at the Cambridge Crystallographic Data Centre and allocated the deposition numbers CCDC 2512443 (**2d** at 100 K), 2512444 (**2d** at 200 K), 2512445 (**2d** at 298 K), 2512446 (**2b** at 100 K), 2512447 (**2f** at 100 K) and 2512448 (**2f** at 298 K).

DFT calculations

All DFT calculations were performed with Amsterdam Modeling Suite software.[104] Geometry optimizations were conducted using ADF2019.307, with the BLYP functional[105] combined with Grimme D3 dispersion correction and the Becke–Johnson damping function,[106–111] along with the TZP basis set with the small frozen core approximation.[112]

In all calculations, scalar relativistic effects were included according to the Zeroth Order Regular Approximation (ZORA).[113–115] The inclusion of scalar relativistic effects was successfully used in mechanistic investigations with compounds containing heavy nuclei.[116–120] When required, solvent effects were incorporated through the COnductor-like Screening MOdel (COSMO), with the default parameters for dichloromethane as implemented in ADF.[121]

All geometry optimizations were therefore performed at the (COSMO)-ZORA-BLYP-D3(BJ)/TZP level of theory. Reactant and product complexes were determined through the Intrinsic Reaction Coordinate (IRC) procedure, as implemented in AMS2020.109. Stationary points were verified by analytical frequency calculations, to confirm that all minima display only positive vibrational frequencies and transition states are associated with a single imaginary frequency.[122–126]

Single-point calculations in solvent were carried out on the optimized geometries to provide a more precise evaluation of electronic energies, using the meta-hybrid M06 functional with the all-electron TZ2P basis set.[127] Gibbs free energies in solution are computed from single-point calculations, accounting for statistical thermodynamics corrections at the standard state (298 K, 1 atm), evaluated at the same level of theory of the optimization procedure. Thus, the level of theory for energy values in this study is denoted as COSMO-ZORA-M06/TZ2P-ae//COSMO-ZORA-BLYP-D3(BJ)/TZP. Both the single-point and the optimization levels of theory were effectively applied in recent studies for the description of palladium–NHC complexes.[27,34,128]

In vitro cytotoxicity

The selected cell lines were grown in accordance with the supplier (Sigma Aldrich) and maintained under a humidified atmosphere with 5% CO_2 at 37 °C. For the *in vitro* cytotoxicity studies, cells were seeded in 96 well-plates (1.0×10^{-3} cells per well for the A2780 cell line, 2.5×10^{-3} cells per well for the A2780*cis* cell line, 2.0×10^{3} cells per well for the OVCAR-5 and KURAMOCHI cell lines, and 8.0×10^{3} cells per well for the MRC-5 cell line) and, after 24 hours, they were treated with increasing concentrations of the organopalladium complexes (0.001, 0.01, 0.1, 1, 10, and 100 μM). For each compound, solutions for the treatment were prepared by appropriate dilution in culture media of a 10 mM stock solution in DMSO. Cisplatin was used as a positive control and applied at the same concentrations as the tested complexes, using an injectable stock solution at concentration 3.33 mM. 96 hours after treatment, the cell viability was assessed using the CellTiter-Glo assay (Promega, Madison, WI, USA) using Tecan M1000 or Synergy^{H1} microplate readers. Dose–response curves for each complex were plotted using GraphPad Prism 8, extrapolating from them the IC_{50} values. For each compound, the final IC_{50} reported is calculated as the average of triplicates and accompanied by the respective standard deviation.

PDTO culture and viability assay

Specimens were completely de-identified prior to use, and consent for research utilization was secured through the biobank at the National Cancer Institute (CRO) in Aviano (approval no. 17197). Cells were isolated from ascites by centrifuging at 1000 rpm for 10 minutes and subsequently washed two times with two cycles of HBSS. Erythrocytes were removed using an erythrocyte lysis solution (Roche Diagnostics, Basel, Switzerland), added while stirring on ice for 10 minutes. Samples were spun again at 1000 rpm for 10 minutes, thus obtaining a cell pellet that was resuspended in Geltrex™ Reduced-Growth Factor Basement-Membrane Matrix (Gibco, Massachusetts, United States).

In the case of solid tumors, samples were incubated for 30 minutes in a mixture of antifungal agents and antibiotics in Dulbecco's Modified Eagle's Medium/Nutrient Mixture F-12 Ham. Incubation was followed by trituration 0.5–1 mm^3 fragments and enzymatic dissociation using a 4 mg mL^{-1} collagenase IV (Gibco, Massachusetts, United States) solution at 37 °C for a maximum of 45 minutes.

The procedure allowed for the obtaining of clusters of cells, which were centrifuged, resuspended in Geltrex™ Reduced-Growth Gactor Basement Membrane Matrix, and finally plated in a 24-well plate. After Geltrex™ solidification, the organoids were maintained in appropriate culture medium as described by Kopper *et al.*[82] and incubated at 37 °C with a 5% CO_2 atmosphere.

In order to assess the anticancer activity of compound **2i**, organoids were seeded in 96-well plates. Clusters of organoids were suspended in Geltrex™ Reduced-Growth Factor Basement Membrane Matrix and a 2 μL drop of this mixture was added to each well. Then, treatment with 6 concentrations of carboplatin, doxorubicin and **2i** was performed; for each of them, four replicates were considered. 96 hours after treatment, the cell viability was assessed using CellTiter-Glo 3D (Promega, Madison, WI, United States). Luminescence signals were acquired using a Synergy^{H1} microplate reader.

Immunofluorescence analyses

The cytochrome-c release and extent of DNA damage were assessed through immunofluorescence assays performed on A2780 cells. In both cases, cells were seeded on a chamber slide with a density of 1×10^{5} cells per well. After 24 hours, each well was treated with compound **2i** (0.5 μM and 1.0 μM) or cisplatin (10 μM), used as positive control, for 3, 6, 24 and 48 hours; a negative control was as well considered for each time-point. Cells were then fixed in 4% paraformaldehyde (DPBS solution; 20 min incubation at RT), permeabilized with 0.3% Triton X-100 (DPBS solution; 15 min incubation at RT) and finally blocked in 8% BSA (DPBS solution, 1 h incubation at RT). Staining with rabbit monoclonal anti-phosphohistone ^{Ser139}p-H2A.X antibody (Cell Signaling Technology, cat. 9718; Danvers, MA) or with mouse monoclonal anticytochrome c antibody (Cell Signaling Technology, cat. 12963; Danvers, MA) was then performed thanks to an overnight incubation of cells at 4 °C with a 1 : 100 diluted solution of each antibody in 1% BSA/DPBS. Cells were then incubated for 1 h with the secondary antibody (Alexa Fluor 488 dye, 1 : 1000 dilution in DPBS, Thermo Fisher Scientific, Invitrogen, cat. # A32723 and # A32731, Waltham, MA) and subsequently nuclei were stained with DAPI 0.1 μg mL^{-1} (DPBS solution, 1 min incubation at RT). Cells were washed three times with DPBS after each incubation step. Finally, each slide was mounted in FluorSave reagent (catalog no. 345789; Millipore: Burlington, MA). Images were acquired using an EVOS FL Auto 2 automated fluorescence microscope (Thermo Fisher Scientific, Waltham, MA, USA).

Inhibition of TrxR

Cell-free TrxR1 inhibition. The assay was performed in 0.2 M Na–K–phosphate buffer pH 7.4, containing 5 mM EDTA, 0.250 mM nicotinamide adenine dinucleotide phosphate (NADPH) and 75 nmol of TrxR1 (IMCO, Sweden) as previously described.[129]

Inhibition of TrxR in ovarian cancer cells. A2780 cells (1×10^{6}) were grown in 75 cm^2 flasks at confluence and treated for 24 h with increasing concentrations of auranofin (range 0.3125–2.5 μM) or **2i** (range 0.625–5 μM). Cell monolayers were harvested, washed with PBS, and centrifuged. Samples were lysed with RIPA buffer (Roche, Basel, Switzerland) and the TrxR assay was performed as above described for isolated enzyme.

Mitochondrial membrane potential ($\Delta\Psi$)

The $\Delta\Psi$ was assayed using the MITO-ID® membrane potential kit according to the manufacturer's instructions (Enzo Life Sciences, Farmingdale, NY).[130] Briefly, A2780 cells (5×10^{3} per

well) were seeded in 96-well plates; after 24 h, the cells were washed with PBS and loaded with MITO-ID detection reagent for 30 min at 37 °C in the dark. Afterwards, the cells were incubated with the tested complexes for 1 or 3 h. Fluorescence intensity was estimated using a plate reader (Fluoroskan Ascent FL, Labsystems, Finland) at 490 (excitation) and 590 nm (emission). Carbonyl cyanide *m*-chlorophenyl hydrazone (CCCP, 3 μM), a chemical inhibitor of oxidative phosphorylation, was used as positive control.

Statistical analysis

All values are the means ± SD of no less than three measurements. Multiple comparisons were made by ANOVA followed by the Tukey–Kramer multiple comparison test (*$p < 0.05$, **$p < 0.01$), using GraphPad software.

Author contributions

Eleonora Botter: conceptualization, investigation, methodology formal analysis and validation of analytical data, visualisation, writing – original draft; Valentina Lauteri: investigation, methodology formal analysis and validation of analytical data; Alessandro Rubbi: conceptualization, investigation, methodology formal analysis and validation of analytical data, visualisation, writing – original draft; Laura Orian: conceptualization, investigation, methodology formal analysis and validation of analytical data, visualisation, writing – original draft; Matteo Forner: investigation, methodology formal analysis and validation of analytical data; Valentina Gandin: conceptualization, investigation, methodology formal analysis and validation of analytical data, visualisation, writing – original draft; Nicola Demitri: data curation, formal analysis, validation and visualisation of X-ray single crystal data; Vincenzo Canzonieri: project administration, resources; Flavio Rizzolio: conceptualization, investigation, methodology formal analysis and validation of analytical data, visualisation, writing – original draft, resources; Enrico Cavarzerani: conceptualization, investigation, methodology formal analysis and validation of analytical data, supervision, project administration, writing – original draft; Fabiano Visentin: conceptualization, investigation, methodology formal analysis and validation of analytical data, supervision, project administration, writing – original draft; Thomas Scattolin: conceptualization, investigation, methodology formal analysis and validation of analytical data, supervision, project administration, writing – original draft.

Conflicts of interest

There are no conflicts to declare.

Data availability

The datasets supporting this article have been uploaded as part of the supplementary information (SI). Supplementary information: experimental procedures, analytical data and spectra. See DOI: https://doi.org/10.1039/d6dt00680a.

CCDC 2512443–2512448 contain the supplementary crystallographic data for this paper.[131a–f]

Acknowledgements

FR was financially supported by the Fondazione AIRC per la Ricerca sul Cancro (grant AIRC IG23566) and VC by the Ministero della Salute – Ricerca Corrente. AR and LO acknowledge funding from the European Union within the MUR PNRR "National Center for HPC, Big Data and Quantum Computing", Mission 4 Component 2 Spoke 8 "*In Silico* Medicine & Ohmics Data" (no. CN0000000013 CN1). All calculations were performed on resources allocated @CINECA (Casalecchio di Reno, Italy) for the project SMART (HP10CDU2JI, P.I.: LO). TS and LO gratefully acknowledge the financial support provided by the Department of Chemical Sciences (PDiSC 2024 project "EasyBackTherapy").

References

1 U. A. Matulonis, A. K. Sood, L. Fallowfield, B. E. Howitt, J. Sehouli and B. Y. Karlan, Ovarian cancer, *Nat. Rev. Dis. Primers*, 2016, **2**, 16061.

2 D. T. Le, J. N. Durham, K. N. Smith, H. Wang, B. R. Bartlett, L. K. Aulakh, S. Lu, H. Kemberling, C. Wilt, B. S. Luber, F. Wong, N. S. Azad, A. A. Rucki, D. Laheru, R. Donehower, A. Zaheer, G. A. Fisher, T. S. Crocenzi, J. J. Lee, T. F. Greten, A. G. Duffy, K. K. Ciombor, A. D. Eyring, B. H. Lam, A. Joe, S. P. Kang, M. Holdhoff, L. Danilova, L. Cope, C. Meyer, S. Zhou, R. M. Goldberg, D. K. Armstrong, K. M. Bever, A. N. Fader, J. Taube, F. Housseau, D. Spetzler, N. Xiao, D. M. Pardoll, N. Papadopoulos, K. W. Kinzler, J. R. Eshleman, B. Vogelstein, R. A. Anders and L. A. Diaz, Mismatch repair deficiency predicts response of solid tumors to PD-1 blockade, *Science*, 2017, **357**, 409–413.

3 U. A. Matulonis, R. Shapira-Frommer, A. D. Santin, A. S. Lisyanskaya, S. Pignata, I. Vergote, F. Raspagliesi, G. S. Sonke, M. Birrer, D. M. Provencher, J. Sehouli, N. Colombo, A. González-Martín, A. Oaknin, P. B. Ottevanger, V. Rudaitis, K. Katchar, H. Wu, S. Keefe, J. Ruman and J. A. Ledermann, Antitumor activity and safety of pembrolizumab in patients with advanced recurrent ovarian cancer: results from the phase II KEYNOTE-100 study, *Ann. Oncol.*, 2019, **30**, 1080–1087.

4 S. Pignata, S. C. Cecere, A. Du Bois, P. Harter and F. Heitz, Treatment of recurrent ovarian cancer, *Ann. Oncol.*, 2017, **28**, viii51–iii56.

5 L. A. Torre, B. Trabert, C. E. DeSantis, K. D. Miller, G. Samimi, C. D. Runowicz, M. M. Gaudet, A. Jemal and R. L. Siegel, Ovarian cancer statistics, *Ca-Cancer J. Clin.*, 2018, **68**, 284–296.

6 Y.-A. Heo, Mirvetuximab Soravtansine: First Approval, *Drugs*, 2023, **83**, 265–273.
7 D. Mauricio, S. Bellone, L. Mutlu, B. McNamara, D. D. Manavella, C. Demirkiran, M. S. Z. Verzosa, N. Buza, P. Hui, T. M. P. Hartwich, J. Harold, Y. Yang-Hartwich, M. Zipponi, G. Altwerger, E. Ratner, G. S. Huang, M. Clark, V. Andikyan, M. Azodi, P. E. Schwartz and A. D. Santin, Trastuzumab deruxtecan (DS-8201a), a HER2-targeting antibody–drug conjugate with topoisomerase I inhibitor payload, shows antitumor activity in uterine and ovarian carcinosarcoma with HER2/neu expression, *Gynecol. Oncol.*, 2023, **170**, 38–45.
8 T. Scattolin, V. A. Voloshkin, F. Visentin and S. P. Nolan, A critical review of palladium organometallic anticancer agents, *Cell Rep. Phys. Sci.*, 2021, **2**, 100446.
9 A. C. F. Caires, Recent Advances Involving Palladium(II) Complexes for the Cancer Therapy, *Anticancer Agents Med. Chem.*, 2007, **7**, 484–491.
10 T. T. Fong, C. Lok, C. Y. Chung, Y. E. Fung, P. Chow, P. Wan and C. Che, Cyclometalated Palladium(II) N–Heterocyclic Carbene Complexes: Anticancer Agents for Potent In Vitro Cytotoxicity and In Vivo Tumor Growth Suppression, *Angew. Chem., Int. Ed.*, 2016, **55**, 11935–11939.
11 A. R. Kapdi and I. J. S. Fairlamb, Anti-cancer palladium complexes: a focus on PdX_2L_2, palladacycles and related complexes, *Chem. Soc. Rev.*, 2014, **43**, 4751–4777.
12 X.-Q. Zhou, M. Xiao, V. Ramu, J. Hilgendorf, X. Li, P. Papadopoulou, M. A. Siegler, A. Kros, W. Sun and S. Bonnet, The Self-Assembly of a Cyclometalated Palladium Photosensitizer into Protein-Stabilized Nanorods Triggers Drug Uptake In Vitro and In Vivo, *J. Am. Chem. Soc.*, 2020, **142**, 10383–10399.
13 A. T. Fiori-Duarte, F. R. G. Bergamini, R. E. F. de Paiva, C. M. Manzano, W. R. Lustri and P. P. Corbi, A new palladium(II) complex with ibuprofen: Spectroscopic characterization, DFT studies, antibacterial activities and interaction with biomolecules, *J. Mol. Struct.*, 2019, **1186**, 144–154.
14 L. Massai, A. Pratesi, J. Bogojeski, M. Banchini, S. Pillozzi, L. Messori and Ž. D. Bugarčić, Antiproliferative properties and biomolecular interactions of three Pd(II) and Pt(II) complexes, *J. Inorg. Biochem.*, 2016, **165**, 1–6.
15 L. Massai, T. Scattolin, M. Tarchi, F. Visentin and L. Messori, Reactions of proteins with a few organopalladium compounds of medicinal interest, *RSC Adv.*, 2022, **12**, 26680–26685.
16 Z. M. Lighvan, H. A. Khonakdar, A. Heydari, M. Rafiee, M. D. Jahromi, A. Derakhshani and A. A. Momtazi-Borojeni, Spectral and molecular docking studies of nucleic acids/protein binding interactions of a novel organometallic palladium(II) complex containing bioactive PTA ligands: Its synthesis, anticancer effects and encapsulation in albumin nanoparticles, *Appl. Organomet. Chem.*, 2020, **34**, e5839.
17 K. Karami, S. Hashemi, J. Lipkowski, F. Mardani, A. A. Momtazi-borojeni and Z. M. Lighvan, Synthesis, characterization and biological activities of two novel orthopalladated complexes: Interactions with DNA and bovine serum albumin, antitumour activity and molecular docking studies, *Appl. Organomet. Chem.*, 2017, **31**, e3740.
18 G. Tonon, M. Mauceri, E. Cavarzerani, R. Piccolo, C. Santo, N. Demitri, L. Orian, P. A. Nogara, J. B. T. Rocha, V. Canzonieri, F. Rizzolio, F. Visentin and T. Scattolin, Unveiling the promising anticancer activity of palladium(II)–aryl complexes bearing diphosphine ligands: a structure–activity relationship analysis, *Dalton Trans.*, 2024, **53**, 8463–8477.
19 F. Bru, M. Vanwynsberghe, E. Botter, G. Tonon, F. Visentin, A. Schiavo, F. Rizzolio, C. S. J. Cazin and T. Scattolin, Synthesis of Gold(I) and Palladium(II) Complexes Bearing *N*-Heterocyclic Carbene Thioglucosides with Selective Cytotoxicity Towards Ovarian Cancer Cells, *Eur. J. Inorg. Chem.*, 2025, **28**, e202400822.
20 X. Wei, Y. Yang, J. Ge, X. Lin, D. Liu, S. Wang, J. Zhang, G. Zhou and S. Li, Synthesis, characterization, DNA/BSA interactions and in vitro cytotoxicity study of palladium(II) complexes of hispolon derivatives, *J. Inorg. Biochem.*, 2020, **202**, 110857.
21 C. Icsel, V. T. Yilmaz, M. Aygun, B. Cevatemre, P. Alper and E. Ulukaya, Palladium(II) and platinum(II) saccharinate complexes with bis(diphenylphosphino)methane/ethane: synthesis, S-phase arrest and ROS-mediated apoptosis in human colon cancer cells, *Dalton Trans.*, 2018, **47**, 11397–11410.
22 T. Scattolin, E. Bortolamiol, F. Visentin, S. Palazzolo, I. Caligiuri, T. Perin, V. Canzonieri, N. Demitri, F. Rizzolio and A. Togni, Palladium(II)-η^3-Allyl Complexes Bearing *N*-Trifluoromethyl *N*-Heterocyclic Carbenes: A New Generation of Anticancer Agents that Restrain the Growth of High-Grade Serous Ovarian Cancer Tumoroids, *Chem. – Eur. J.*, 2020, **26**, 11868–11876.
23 E. Bortolamiol, M. Mauceri, R. Piccolo, E. Cavarzerani, N. Demitri, C. Donati, V. Gandin, S. K. Brezar, U. Kamensek, M. Cemazar, V. Canzonieri, F. Rizzolio, F. Visentin and T. Scattolin, Palladium(II)-Indenyl Complexes Bearing N-Heterocyclic Carbene (NHC) Ligands as Potent and Selective Metallodrugs toward High-Grade Serous Ovarian Cancer Models, *J. Med. Chem.*, 2024, **67**, 14414–14431.
24 E. Bortolamiol, F. Fama, Z. Zhang, N. Demitri, L. Cavallo, I. Caligiuri, F. Rizzolio, T. Scattolin and F. Visentin, Cationic palladium(II)-indenyl complexes bearing phosphines as ancillary ligands: synthesis, and study of indenyl amination and anticancer activity, *Dalton Trans.*, 2022, **51**, 11135–11151.
25 T. Scattolin, E. Bortolamiol, S. Palazzolo, I. Caligiuri, T. Perin, V. Canzonieri, N. Demitri, F. Rizzolio, L. Cavallo, B. Dereli, M. V. Mane, S. P. Nolan and F. Visentin, The anticancer activity of an air-stable Pd(I)-NHC (NHC = N-heterocyclic carbene) dimer, *Chem. Commun.*, 2020, **56**, 12238–12241.

26 C. Donati, I. I. Hashim, N. B. Pozsoni, L. Bourda, K. Van Hecke, C. S. J. Cazin, F. Visentin, S. P. Nolan, V. Gandin and T. Scattolin, Investigation of the *in vitro* anticancer potential of bis(imino)acenaphthene–N-heterocyclic carbene transition metal complexes revealed TrxR inhibition and triggering of immunogenic cell death (ICD) for allyl palladates, *RSC Med. Chem.*, 2025, **16**, 2592–2602.

27 T. Scattolin, I. Pessotto, E. Cavarzerani, V. Canzonieri, L. Orian, N. Demitri, C. Schmidt, A. Casini, E. Bortolamiol, F. Visentin, F. Rizzolio and S. P. Nolan, Indenyl and Allyl Palladate Complexes Bearing *N*-Heterocyclic Carbene Ligands: an Easily Accessible Class of New Anticancer Drug Candidates, *Eur. J. Inorg. Chem.*, 2022, **2022**, e202200103.

28 T. Scattolin, E. Bortolamiol, F. Rizzolio, N. Demitri and F. Visentin, Allyl palladium complexes bearing carbohydrate–based *N*-heterocyclic carbenes: Anticancer agents for selective and potent *in vitro* cytotoxicity, *Appl. Organomet. Chem.*, 2020, **34**, e5876.

29 R. Saito, P. Arnaut, B. Maliszewski, L. Tripodi, I. Caligiuri, F. Rizzolio, T. Scattolin and S. P. Nolan, Facile and green synthesis of [Pd(NHC)(η^3-R-allyl)Cl] complexes and their anticancer activity, *Dalton Trans.*, 2025, **54**, 11720–11724.

30 T. Scattolin, S. Giust, P. Bergamini, I. Caligiuri, L. Canovese, N. Demitri, R. Gambari, I. Lampronti, F. Rizzolio and F. Visentin, Palladacyclopentadienyl complexes bearing purine–based N–heterocyclic carbenes: A new class of promising antiproliferative agents against human ovarian cancer, *Appl. Organomet. Chem.*, 2019, **33**, e4902.

31 T. Scattolin, I. Caligiuri, N. Mouawad, M. El Boustani, N. Demitri, F. Rizzolio and F. Visentin, Synthesis and in-depth studies on the anticancer activity of novel palladacyclopentadienyl complexes stabilized by *N*-Heterocyclic carbene ligands, *Eur. J. Med. Chem.*, 2019, **179**, 325–334.

32 R. Gencheva and E. S. J. Arnér, Thioredoxin Reductase Inhibition for Cancer Therapy, *Annu. Rev. Pharmacol. Toxicol.*, 2022, **62**, 177–196.

33 H. Ghareeb and N. Metanis, The Thioredoxin System: A Promising Target for Cancer Drug Development, *Chem. – Eur. J.*, 2020, **26**, 10175–10184.

34 A. Madabeni, T. Scattolin, E. Bortolamiol, F. Visentin and L. Orian, Reactivity of Palladium(II)-η^3 -Allyl Complexes with Chalcogenolates: A Density Functional Study of Their Antitumor Implications, *Organometallics*, 2024, **43**, 954–962.

35 B. M. Trost and T. J. Fullerton, New synthetic reactions. Allylic alkylation, *J. Am. Chem. Soc.*, 1973, **95**, 292–294.

36 A. C. Tsipis, NMR probe effects on *trans*-philicity and *trans*-influence ladders in square planar Pt(ii) complexes, *New J. Chem.*, 2020, **44**, 7976–7986.

37 J. N. Crosby and R. D. W. Kemmitt, The interaction of tin (II) chloride with some allyl complexes of platinum and palladium and diene complexes of rhodium, *J. Organomet. Chem.*, 1971, **26**, 277–284.

38 U. Belluco, G. Deganello, R. Pietropaolo and P. Uguagliati, Complexes of Platinum(II) with group IV donor ligands, *Inorg. Chim. Acta, Rev.*, 1970, **4**, 7–39.

39 A. Albinati, P. S. Pregosin and H. Ruegger, Trichlorostannate Complexes of Platinum. Synthesis, Multinuclear NMR Spectroscopy and X-Ray Crystallography of *trans*-[$Pt(SnCl_3)_2(P(OPh)_3)_2$] and Related Complexes, *Inorg. Chem.*, 1984, **23**, 3223–3229.

40 A. Musco, R. Pontellini, M. Grassi, A. Sironi, S. V. Meille, H. Ruegger, C. Ammann and P. S. Pregosin, Crystallographic and NMR studies of platinum(II) and palladium(II) η^3-methallyl trichlorostannate olefin complexes, *Organometallics*, 1988, **7**, 2130–2137.

41 M. Grassi, S. V. Meille, A. Musco, R. Pontellini and A. Sironi, Crystallographic and nuclear magnetic resonance studies of carbonyl(η^3-methylallyl)(trichlorostannyl) complexes of platinum(II) and palladium(II), *J. Chem. Soc., Dalton Trans.*, 1989, 615–621.

42 M. Grassi, S. V. Meille, A. Musco, R. Pontellini and A. Sironi, Palladium(II) and platinum(II) η^3-methylallyl trichlorotin complexes. Part 3. Crystal structure analysis of [$Pt(\eta^3$-$C_4H_7)(cod)]_2[Pt(\eta^3$-$C_4$ $H_7)(SnCl_3)_3$](cod = cyclo-octa-1,5-diene), *J. Chem. Soc., Dalton Trans.*, 1990, 251–255.

43 V. García, M. A. Garralda and L. Ibarlucea, Rhodium(I) complexes with bidentate nitrogen heterocycles and their reactions with tin(II) chloride and carbon monoxide, *Transition Met. Chem.*, 1985, **10**, 288–291.

44 S. G. Bott, J. C. Machell, D. M. P. Mingos and M. J. Watson, Synthesis and structural characterisation of the complex *mer*-[{$Rh(CNC_8H_9)_3(SnCl_3)(\mu$-$SnCl_2)$}$_2$], *J. Chem. Soc., Dalton Trans.*, 1991, 859–862.

45 M. T. Pinillos, A. Elduque, J. A. López, F. J. Lahoz, L. A. Oro and B. E. Mann, Reactivity of binuclear heterobridged iridium complexes with $SnCl_2$, *J. Chem. Soc., Dalton Trans.*, 1992, 2389–2393.

46 A. K. Maity, M. Bhattacharjee and S. Roy, $SnCl_2$ insertion into Ir–Cl and Rh–Cl bonds: Synthesis, characterization and catalytic activity of three-legged piano-stool trichlorostannyl iridium and rhodium complexes, *J. Organomet. Chem.*, 2014, **768**, 42–49.

47 M. Kretschmer and P. S. Pregosin, ^{1}H, ^{31}P and ^{119}Sn NMR studies of iridium trichlorostannate complexes, *Inorg. Chim. Acta*, 1982, **61**, 247–254.

48 B. Therrien, T.-T. Thai, J. Freudenreich, G. Süss-Fink, S. S. Shapovalov, A. A. Pasynskii and L. Plasseraud, Bimetallic ruthenium–tin chemistry: Synthesis and molecular structure of arene ruthenium complexes containing trichlorostannyl ligands, *J. Organomet. Chem.*, 2010, **695**, 409–414.

49 M. Novák, M. Bouška, L. Dostál, M. Lutter, K. Jurkschat, J. Turek, F. De Proft, Z. Růžičková and R. Jambor, Role of the Trichlorostannyl Ligand in Tin–Ruthenium Arene Complexes: Experimental and Computational Studies, *Eur. J. Inorg. Chem.*, 2017, **2017**, 1292–1300.

50 O. Renier, C. Deacon-Price, J. Peters, K. Nurekeyeva, C. Russon, S. Dyson, S. Ngubane, J. Baumgartner, P. Dyson, T. Riedel, H. Chiririwa and B. Blom, Synthesis and In Vitro (Anticancer) Evaluation of η^6-Arene Ruthenium Complexes Bearing Stannyl Ligands, *Inorganics*, 2017, **5**, 44.

51 N. Álvarez-Pazos, G. Albertin, S. Antoniutti, J. Bravo, S. García-Fontán, J. M. Hermida-Ramón and G. Zanardo, Trichlorostannyl complexes of Ruthenium(II): Synthesis, structure, reactivity and computational studies, *J. Organomet. Chem.*, 2018, **874**, 74–82.

52 C. Berg, S. Chari, K. Jurgaityte, A. Laurora, M. Naldony, F. Pope, D. Romano, T. Medupe, S. Prince, S. Ngubane, J. Baumgartner and B. Blom, Modulation of the solubility properties of arene ruthenium complexes bearing stannyl ligands as potential anti-cancer agents, *J. Organomet. Chem.*, 2019, **891**, 12–19.

53 G. Albertin, S. Antoniutti and J. Castro, Reactivity of Dihydrides MH_2P_4(M = Fe, Ru, Os) with $SnCl_2$: Preparation of Bis(trihydridestannyl) Derivatives, *Organometallics*, 2010, **29**, 3808–3816.

54 T. Nabiyeva, B. Roufosse, M. Odachowski, J. Baumgartner, C. Marschner, A. K. Verma and B. Blom, Osmium Arene Germyl, Stannyl, Germanate, and Stannate Complexes as Anticancer Agents, *ACS Omega*, 2021, **6**, 19252–19268.

55 S. Latiş, C. Marschner, J. Baumgartner, S. Prince, S. Biswas, S. Chakraborty, K. G. Garcia, R. M. A. Heeren, S. Van Nuffel and B. Blom, Synthesis and in vitro anticancer studies of arene ruthenium(II) and arene osmium(II) complexes bearing arsine and stibine co-ligands on breast cancer cell-lines, *J. Organomet. Chem.*, 2023, **1001**, 122891.

56 S. N. Syed Annuar, N. F. Kamaludin, N. Awang and K. M. Chan, Cellular Basis of Organotin(IV) Derivatives as Anticancer Metallodrugs: A Review, *Front. Chem.*, 2021, **9**, 657599.

57 J. Wu, T. Yang, X. Wang, W. Li, M. Pang, H. Sun, H. Liang and F. Yang, Development of a multi-target anticancer Sn (ii) pyridine-2-carboxaldehyde thiosemicarbazone complex, *Dalton Trans.*, 2021, **50**, 10909–10921.

58 P. Köpf-Maier, C. Janiak and H. Schumann, Antitumor properties of organometallic metallocene complexes of tin and germanium, *J. Cancer Res. Clin. Oncol.*, 1988, **114**, 502–506.

59 B. Z. Momeni, L. J. Baleh, S. Hamzeh and F. Rominger, Insertion of $SnCl_2$ into Pt–Cl bonds: synthesis and characterization of four- and five-coordinate trichlorostannylplatinum(II) complexes, *J. Coord. Chem.*, 2007, **60**, 285–293.

60 S. H. L. Thoonen, M. Lutz, A. L. Spek, B.-J. Deelman and G. Van Koten, Synthesis of Novel Trialkyl(trichlorostannyl) platinum(IV) Complexes through $SnCl_2$ Insertion into the Pt–Cl Bond, *Organometallics*, 2003, **22**, 1156–1159.

61 B. Alvarez, D. Miguel, J. A. Pérez-Martinez, V. Riera and S. García-Granda, The first examples of insertion of $SnCl_2$ into the Mn-Cl and Re-Cl bonds of octahedral complexes: X-ray structure of $[Mn(CO)_3(SnCl_3)(S_2CPCy_3)]\cdot CH_2Cl_2$, *J. Organomet. Chem.*, 1992, **427**, C33–C36.

62 M. Noskowska, E. Śliwińska and W. Duczmal, Simple fast preparation of neutral palladium(II) complexes with $SnCl^-_3$ and Cl^- ligands, *Transition Met. Chem.*, 2003, **28**, 756–759.

63 M. Gianotti, A. Musco, M. Sisti, M. Grassi and G. Gatti, The Dynamic Behaviour of η^3-Allyl Palladium and Platinum Complexes Containing the $SnCl_3$ Ligand, *Inorg. Chim. Acta*, 1987, **133**, 255–259.

64 K. Hirako, Y. Miyamoto, K. Kakiuchi and H. Kurosawa, Formation of an allyl-tin bond in η^3-allyl(trichlorostannyl) palladium(II) complexes, *Inorg. Chim. Acta*, 1994, **222**, 21–25.

65 A. Van Niekerk, P. Chellan and S. F. Mapolie, Heterometallic Multinuclear Complexes as Anti–Cancer Agents–An Overview of Recent Developments, *Eur. J. Inorg. Chem.*, 2019, **2019**, 3432–3455.

66 N. Curado and M. Contel, in *Metal-based Anticancer Agents*, ed. A. Casini, A. Vessières and S. M. Meier-Menches, The Royal Society of Chemistry, 2019, pp. 143–168.

67 M. C. Dietl, M. Maag, S. Ber, F. Rominger, M. Rudolph, I. Caligiuri, P. K. Andele, I. A. I. Mkhalid, F. Rizzolio, P. A. Nogara, L. Orian, T. Scattolin and A. S. K. Hashmi, Comparative study of the antiproliferative activity of heterometallic carbene gold(I)–platinum(II) and gold(I)–palladium(II) complexes in cancer cell lines, *Chem. Sci.*, 2024, **15**, 15291–15298.

68 T. Scattolin, A. A. Logvinov, N. V. Tzouras, C. S. J. Cazin and S. P. Nolan, Advances in the Synthesis and Applications of *N*-Heterocyclic Carbene Metal Complexes with a Focus on the Weak Base Route, *Organometallics*, 2023, **42**, 2692–2730.

69 L. Canovese, F. Visentin, C. Levi and A. Dolmella, Synthesis, characterization, dynamics and reactivity toward amination of η^3-allyl palladium complexes bearing mixed ancillary ligands. evaluation of the electronic characteristics of the ligands from kinetic data, *Dalton Trans.*, 2011, **40**, 966–981.

70 S. Sakaki, K. Takeuchi, M. Sugimoto and H. Kurosawa, Geometries, Bonding Nature, and Relative Stabilities of Dinuclear Palladium(I) π-Allyl and Mononuclear Palladium(II) π-Allyl Complexes. A Theoretical Study, *Organometallics*, 1997, **16**, 2995–3003.

71 L. Canovese, F. Visentin, P. Uguagliati, V. Lucchini and G. Bandoli, Crystal structure and fluxional behavior of novel Pd(II) allyl complexes containing a potentially tridentate S,N,S ligand: an example of selective *syn-anti* isomerism, *Inorg. Chim. Acta*, 1998, **277**, 247–252.

72 M. B. Abrams, J. C. Yoder, C. Loeber, M. W. Day and J. E. Bercaw, Fluxional η^3-Allyl Derivatives of ansa-Scandocenes and an ansa-Yttrocene. Measurements of the Barriers for the η^3 to η^1 Process as an Indicator of Olefin Binding Energy to d^0 Metallocenes, *Organometallics*, 1999, **18**, 1389–1401.

73 R. Benn, A. Rufińska and G. Schroth, Fluxional behaviour in η^3-allyl complexes of cr, mo and w as shown by magnetisation transfer difference spectroscopy (MTDS), *J. Organomet. Chem.*, 1981, **217**, 91–104.

74 J. Y. Wang, A. E. Strom and J. F. Hartwig, Mechanistic Studies of Palladium-Catalyzed Aminocarbonylation of Aryl Chlorides with Carbon Monoxide and Ammonia, *J. Am. Chem. Soc.*, 2018, **140**, 7979–7993.

75 M. K. Nayak, A. Mohanty and S. Roy, NHC as a Ligand in Heterobimetallic Catalysis: An Insight into a Catalytic Friedel–Crafts-like Reaction, *Organometallics*, 2023, **42**, 1927–1933.
76 N. Marion, O. Navarro, J. Mei, E. D. Stevens, N. M. Scott and S. P. Nolan, Modified (NHC)Pd(allyl)Cl (NHC = N-Heterocyclic Carbene) Complexes for Room-Temperature Suzuki–Miyaura and Buchwald–Hartwig Reactions, *J. Am. Chem. Soc.*, 2006, **128**, 4101–4111.
77 T. Scattolin, I. Caligiuri, L. Canovese, N. Demitri, R. Gambari, I. Lampronti, F. Rizzolio, C. Santo and F. Visentin, Synthesis of new allyl palladium complexes bearing purine-based NHC ligands with antiproliferative and proapoptotic activities on human ovarian cancer cell lines, *Dalton Trans.*, 2018, **47**, 13616–13630.
78 T. Scattolin, A. Piccin, M. Mauceri, F. Rizzolio, N. Demitri, V. Canzonieri and F. Visentin, Synthesis, characterization and anticancer activity of palladium allyl complexes bearing benzimidazole-based N-heterocyclic carbene (NHC) ligands, *Polyhedron*, 2021, **207**, 115381.
79 T. Scattolin, G. Andreetta, M. Mauceri, F. Rizzolio, N. Demitri, V. Canzonieri and F. Visentin, Imidazo[1,5-a]pyridine-3-ylidenes and dipyridoimidazolinylidenes as ancillary ligands in Palladium allyl complexes with potent *in vitro* anticancer activity, *J. Organomet. Chem.*, 2021, **952**, 122014.
80 T. Scattolin, N. Pangerc, I. Lampronti, C. Tupini, R. Gambari, L. Marvelli, F. Rizzolio, N. Demitri, L. Canovese and F. Visentin, Palladium (0) olefin complexes bearing purine-based *N*-heterocyclic carbenes and 1,3,5-triaza-7-phosphaadamantane (PTA): Synthesis, characterization and antiproliferative activity toward human ovarian cancer cell lines, *J. Organomet. Chem.*, 2019, **899**, 120857.
81 J. Kalla, J. Pfneissl, T. Mair, L. Tran and G. Egger, A systematic review on the culture methods and applications of 3D tumoroids for cancer research and personalized medicine, *Cell. Oncol.*, 2025, **48**, 1–26.
82 O. Kopper, C. J. De Witte, K. Lõhmussaar, J. E. Valle-Inclan, N. Hami, L. Kester, A. V. Balgobind, J. Korving, N. Proost, H. Begthel, L. M. Van Wijk, S. A. Revilla, R. Theeuwsen, M. Van De Ven, M. J. Van Roosmalen, B. Ponsioen, V. W. H. Ho, B. G. Neel, T. Bosse, K. N. Gaarenstroom, H. Vrieling, M. P. G. Vreeswijk, P. J. Van Diest, P. O. Witteveen, T. Jonges, J. L. Bos, A. Van Oudenaarden, R. P. Zweemer, H. J. G. Snippert, W. P. Kloosterman and H. Clevers, An organoid platform for ovarian cancer captures intra- and interpatient heterogeneity, *Nat. Med.*, 2019, **25**, 838–849.
83 K. F. Idrisova, H.-U. Simon and M. O. Gomzikova, Role of Patient-Derived Models of Cancer in Translational Oncology, *Cancers*, 2023, **15**, 139.
84 H. Yang, Y. Wang, P. Wang, N. Zhang and P. Wang, Tumor organoids for cancer research and personalized medicine, *Cancer Biol. Med.*, 2022, **19**, 319–332.
85 Y.-H. Lo, K. Karlsson and C. J. Kuo, Applications of organoids for cancer biology and precision medicine, *Nat. Cancer*, 2020, **1**, 761–773.
86 T. Takahashi, Organoids for Drug Discovery and Personalized Medicine, *Annu. Rev. Pharmacol. Toxicol.*, 2019, **59**, 447–462.
87 E. J. Anthony, E. M. Bolitho, H. E. Bridgewater, O. W. L. Carter, J. M. Donnelly, C. Imberti, E. C. Lant, F. Lermyte, R. J. Needham, M. Palau, P. J. Sadler, H. Shi, F.-X. Wang, W.-Y. Zhang and Z. Zhang, Metallodrugs are unique: opportunities and challenges of discovery and development, *Chem. Sci.*, 2020, **11**, 12888–12917.
88 M. Ott, J. D. Robertson, V. Gogvadze, B. Zhivotovsky and S. Orrenius, Cytochrome c release from mitochondria proceeds by a two-step process, *Proc. Natl. Acad. Sci. U. S. A.*, 2002, **99**, 1259–1263.
89 I. H. Ismail, T. I. Wadhra and O. Hammarsten, An optimized method for detecting gamma-H2AX in blood cells reveals a significant interindividual variation in the gamma-H2AX response among humans, *Nucleic Acids Res.*, 2007, **35**, e36.
90 M. Fragkos, J. Jurvansuu and P. Beard, H2AX Is Required for Cell Cycle Arrest via the p53/p21 Pathway, *Mol. Cell. Biol.*, 2009, **29**, 2828–2840.
91 D. B. G. Williams and M. Lawton, Drying of Organic Solvents: Quantitative Evaluation of the Efficiency of Several Desiccants, *J. Org. Chem.*, 2010, **75**, 8351–8354.
92 T. Scattolin, P. Lippmann, M. Beliš, K. Van Hecke, I. Ott and S. P. Nolan, A simple synthetic entryway into (*N*-heterocyclic carbene)gold–steroidyl complexes and their anticancer activity, *Appl. Organomet. Chem.*, 2024, **38**, e6624.
93 C. Cesari, S. Conti, S. Zacchini, V. Zanotti, M. C. Cassani and R. Mazzoni, Sterically driven synthesis of ruthenium and ruthenium–silver N-heterocyclic carbene complexes, *Dalton Trans.*, 2014, **43**, 17240–17243.
94 H.-L. Su, L. M. Pérez, S.-J. Lee, J. H. Reibenspies, H. S. Bazzi and D. E. Bergbreiter, Studies of Ligand Exchange in N-Heterocyclic Carbene Silver(I) Complexes, *Organometallics*, 2012, **31**, 4063–4071.
95 R. P. Hegde, N. Demitri, A. Héroux, A. Olivo, G. Bais, M. Cianci, P. Storici, D.-G. Dumitrescu, N. K. Varshney, B. Gopal, D. D. Sarma, L. Vaccari, S. Onesti and M. Polentarutti, Macromolecular crystallography at Elettra: current and future perspectives, *J. Synchrotron Radiat.*, 2025, **32**, 757–765.
96 W. Kabsch, XDS, *Acta Crystallogr., Sect. D: Biol. Crystallogr.*, 2010, **66**, 125–132.
97 M. D. Winn, C. C. Ballard, K. D. Cowtan, E. J. Dodson, P. Emsley, P. R. Evans, R. M. Keegan, E. B. Krissinel, A. G. W. Leslie, A. McCoy, S. J. McNicholas, G. N. Murshudov, N. S. Pannu, E. A. Potterton, H. R. Powell, R. J. Read, A. Vagin and K. S. Wilson, Overview of the CCP4 suite and current developments, *Acta Crystallogr., Sect. D: Biol. Crystallogr.*, 2011, **67**, 235–242.
98 P. R. Evans and G. N. Murshudov, How good are my data and what is the resolution?, *Acta Crystallogr., Sect. D: Biol. Crystallogr.*, 2013, **69**, 1204–1214.

99 G. M. Sheldrick, SHELXT – Integrated space-group and crystal-structure determination, *Acta Crystallogr., Sect. A: Found. Adv.*, 2015, **71**, 3–8.
100 G. M. Sheldrick, Crystal structure refinement with SHELXL, *Acta Crystallogr., Sect. C*, 2015, **71**, 3–8.
101 P. Emsley, B. Lohkamp, W. G. Scott and K. Cowtan, Features and development of Coot, *Acta Crystallogr., Sect. D: Biol. Crystallogr.*, 2010, **66**, 486–501.
102 L. J. Farrugia, WinGX and ORTEP for Windows: an update, *J. Appl. Crystallogr.*, 2012, **45**, 849–854.
103 PyMOL | pymol.org, https://www.pymol.org/, (accessed 12 December 2025).
104 E. J. Baerends, N. F. Aguirre, N. D. Austin, J. Autschbach, F. M. Bickelhaupt, R. Bulo, C. Cappelli, A. C. T. Van Duin, F. Egidi, C. Fonseca Guerra, A. Förster, M. Franchini, T. P. M. Goumans, T. Heine, M. Hellström, C. R. Jacob, L. Jensen, M. Krykunov, E. Van Lenthe, A. Michalak, M. M. Mitoraj, J. Neugebauer, V. P. Nicu, P. Philipsen, H. Ramanantoanina, R. Rüger, G. Schreckenbach, M. Stener, M. Swart, J. M. Thijssen, T. Trnka, L. Visscher, A. Yakovlev and S. Van Gisbergen, The Amsterdam Modeling Suite, *J. Chem. Phys.*, 2025, **162**, 162501.
105 P. M. W. Gill, B. G. Johnson, J. A. Pople and M. J. Frisch, The performance of the Becke—Lee—Yang—Parr (B—LYP) density functional theory with various basis sets, *Chem. Phys. Lett.*, 1992, **197**, 499–505.
106 S. Grimme, Density functional theory with London dispersion corrections, *Wiley Interdiscip. Rev.: Comput. Mol. Sci.*, 2011, **1**, 211–228.
107 S. Grimme, J. Antony, S. Ehrlich and H. Krieg, A consistent and accurate *ab initio* parametrization of density functional dispersion correction (DFT-D) for the 94 elements H-Pu, *J. Chem. Phys.*, 2010, **132**, 154104.
108 A. D. Becke and E. R. Johnson, Exchange-hole dipole moment and the dispersion interaction, *J. Chem. Phys.*, 2005, **122**, 154104.
109 A. D. Becke and E. R. Johnson, A density-functional model of the dispersion interaction, *J. Chem. Phys.*, 2005, **123**, 154101.
110 E. R. Johnson and A. D. Becke, A post-Hartree–Fock model of intermolecular interactions, *J. Chem. Phys.*, 2005, **123**, 024101.
111 S. Grimme, S. Ehrlich and L. Goerigk, Effect of the damping function in dispersion corrected density functional theory, *J. Comput. Chem.*, 2011, **32**, 1456–1465.
112 E. Van Lenthe and E. J. Baerends, Optimized Slater–type basis sets for the elements 1–118, *J. Comput. Chem.*, 2003, **24**, 1142–1156.
113 E. V. Lenthe, E. J. Baerends and J. G. Snijders, Relativistic regular two-component Hamiltonians, *J. Chem. Phys.*, 1993, **99**, 4597–4610.
114 E. Van Lenthe, E. J. Baerends and J. G. Snijders, Relativistic total energy using regular approximations, *J. Chem. Phys.*, 1994, **101**, 9783–9792.
115 E. Van Lenthe, A. Ehlers and E.-J. Baerends, Geometry optimizations in the zero order regular approximation for relativistic effects, *J. Chem. Phys.*, 1999, **110**, 8943–8953.
116 M. Bortoli, S. M. Ahmad, T. A. Hamlin, F. M. Bickelhaupt and L. Orian, Nature and strength of chalcogen–π bonds, *Phys. Chem. Chem. Phys.*, 2018, **20**, 27592–27599.
117 A. Madabeni, P. A. Nogara, M. Bortoli, J. B. T. Rocha and L. Orian, Effect of Methylmercury Binding on the Peroxide-Reducing Potential of Cysteine and Selenocysteine, *Inorg. Chem.*, 2021, **60**, 4646–4656.
118 D. Zeppilli, A. Madabeni, L. Sancineto, L. Bagnoli, C. Santi and L. Orian, Role of Group 12 Metals in the Reduction of H_2O_2 by Santi's Reagent: A Computational Mechanistic Investigation, *Inorg. Chem.*, 2023, **62**, 17288–17298.
119 A. Madabeni, D. Tanini, A. Capperucci and L. Orian, Untangling the catalytic importance of the Se oxidation state in organoselenium-mediated oxygen-transfer reactions: the conversion of aniline to nitrobenzene, *Chem. Sci.*, 2024, **15**, 12126–12137.
120 A. Rubbi, D. Tanini, A. Capperucci and L. Orian, Glutathione Peroxidase-Like Activity of Functionalized Tellurides: Insights into the Oxidation Mechanism Through Activation Strain Analysis, *Inorg. Chem.*, 2025, **64**, 10022–10031.
121 C. C. Pye and T. Ziegler, An implementation of the conductor-like screening model of solvation within the Amsterdam density functional package, *Theor. Chem. Acc.*, 1999, **101**, 396–408.
122 L. Versluis and T. Ziegler, The determination of molecular structures by density functional theory. The evaluation of analytical energy gradients by numerical integration, *J. Chem. Phys.*, 1988, **88**, 322–328.
123 L. Fan and T. Ziegler, Nonlocal density functional theory as a practical tool in calculations on transition states and activation energies. Applications to elementary reaction steps in organic chemistry, *J. Am. Chem. Soc.*, 1992, **114**, 10890–10897.
124 A. Bérces, R. M. Dickson, L. Fan, H. Jacobsen, D. Swerhone and T. Ziegler, An implementation of the coupled perturbed Kohn-Sham equations: perturbation due to nuclear displacements, *Comput. Phys. Commun.*, 1997, **100**, 247–262.
125 H. Jacobsen, A. Bérces, D. P. Swerhone and T. Ziegler, Analytic second derivatives of molecular energies: a density functional implementation, *Comput. Phys. Commun.*, 1997, **100**, 263–276.
126 S. K. Wolff, Analytical second derivatives in the Amsterdam density functional package, *Int. J. Quantum Chem.*, 2005, **104**, 645–659.
127 Y. Zhao and D. G. Truhlar, The M06 suite of density functionals for main group thermochemistry, thermochemical kinetics, noncovalent interactions, excited states, and transition elements: two new functionals and systematic testing of four M06-class functionals and 12 other functionals, *Theor. Chem. Acc.*, 2008, **120**, 215–241.
128 M. Monticelli, M. Baron, C. Tubaro, S. Bellemin-Laponnaz, C. Graiff, G. Bottaro, L. Armelao and L. Orian,

Structural and Luminescent Properties of Homoleptic Silver(I), Gold(I), and Palladium(II) Complexes with *n*NHC-*tz*NHC Heteroditopic Carbene Ligands, *ACS Omega*, 2019, **4**, 4192–4205.

129 A. Zanella, V. Gandin, M. Porchia, F. Refosco, F. Tisato, F. Sorrentino, G. Scutari, M. P. Rigobello and C. Marzano, Cytotoxicity in human cancer cells and mitochondrial dysfunction induced by a series of new copper(I) complexes containing tris(2-cyanoethyl)phosphines, *Invest. New Drugs*, 2011, **29**, 1213–1223.

130 F. Miglioli, M. De Franco, J. Bartoli, M. Scaccaglia, G. Pelosi, C. Marzano, D. Rogolino, V. Gandin and M. Carcelli, Anticancer activity of new water-soluble sulfonated thiosemicarbazone copper(II) complexes targeting disulfide isomerase, *Eur. J. Med. Chem.*, 2024, **276**, 116697.

131 (*a*) CCDC 2512443: Experimental Crystal Structure Determination, 2026, DOI: 10.5517/ccdc.csd.cc2qbdk1; (*b*) CCDC 2512444: Experimental Crystal Structure Determination, 2026, DOI: 10.5517/ccdc.csd.cc2qbdl2; (*c*) CCDC 2512445: Experimental Crystal Structure Determination, 2026, DOI: 10.5517/ccdc.csd.cc2qbdm3; (*d*) CCDC 2512446: Experimental Crystal Structure Determination, 2026, DOI: 10.5517/ccdc.csd.cc2qbdn4; (*e*) CCDC 2512447: Experimental Crystal Structure Determination, 2026, DOI: 10.5517/ccdc.csd.cc2qbdp5; (*f*) CCDC 2512448: Experimental Crystal Structure Determination, 2026, DOI: 10.5517/ccdc.csd.cc2qbdq6.